The Santa Ana winds of Southern California: Winds, gusts, and the 2007 Witch fire

Robert G. Fovell[*1] and Yang Cao[2]

[1]*Department of Atmospheric and Environmental Sciences, University at Albany, State University of New York, Albany, NY, USA*
[2]*Department of Hydrology and Atmospheric Sciences, The University of Arizona, Tucson, AZ, USA*

Abstract. The Santa Ana winds occur in Southern California during the September-May time frame, bringing low humidities across the area and strong winds at favored locations, which include some mountain gaps and on particular slopes. The exceptionally strong event of late October 2007, which sparked and/or spread numerous fires across the region, is compared to more recent events using a numerical model verified against a very dense, limited-area network (mesonet) that has been recently deployed in San Diego County. The focus is placed on the spatial and temporal structure of the winds within the lowest two kilometers above the ground within the mesonet, along with an attempt to gauge winds and gusts occurring during and after the onset of October 2007's Witch fire, which became one of the largest wildfires in California history.

Keywords: complex terrain; downslope winds; numerical weather prediction; gust forecasting

1. Introduction

The "Santa Ana" is a dry, sometimes hot, offshore[*] wind directed from the Great Basin and Mojave Desert (Fig. 1) over the mountains and through the passes of Southern California (Sommers 1978, Small 1995). Its season is often thought of as extending from September to April (Raphael 2003), although prominent May events have occurred in recent years. At various places in the Los Angeles basin, fast winds are associated with terrain gaps and/or particular mountain slopes (Huang *et al*. 2009, Hughes and Hall 2010, Cao and Fovell 2016), resulting in both wind corridors and shadows. Although some attention has been paid to the phenomenon (Conil and Hall 2006, Jones *et al*. 2010), the literature on the subject is surprisingly thin given the meteorological and economic importance of the winds.

In particular, the fast winds combine with low relative humidities to produce substantial fire danger, especially in the autumn season before the winter rains have begun (Sommers 1978, Westerling *et al*. 2004). Chang and Schoenberg (2011) showed that while fires occur through the year in Los Angeles, large fires cluster in the September-November time frame (see their Fig. 2).

---

*Corresponding author, Professor, E-mail: rfovell@albany.edu
[*] In meteorology, winds are identified by their origin, so an "offshore" wind blows from land towards sea, in contrast to an "onshore" wind, or sea-breeze.

On 21 October 2007, at or before 1930 UTC (1230 local daylight time), the Witch Creek fire started at 33.083083°N, 116.694139°W in San Diego County[†], one of more than two dozen Southern California blazes driven by an especially strong Santa Ana wind event. High winds can damage electrical transmission poles and/or wires (e.g., Aboshosha and El Damatty 2015, Yang and Zhang 2016, Lou *et al*. 2016) and, in this case, ignition was apparently caused by the wind-induced faulting (arcing) of power lines located roughly 20 m above ground level (AGL). The fire spread rapidly and merged with other blazes, becoming one of the largest in California history.
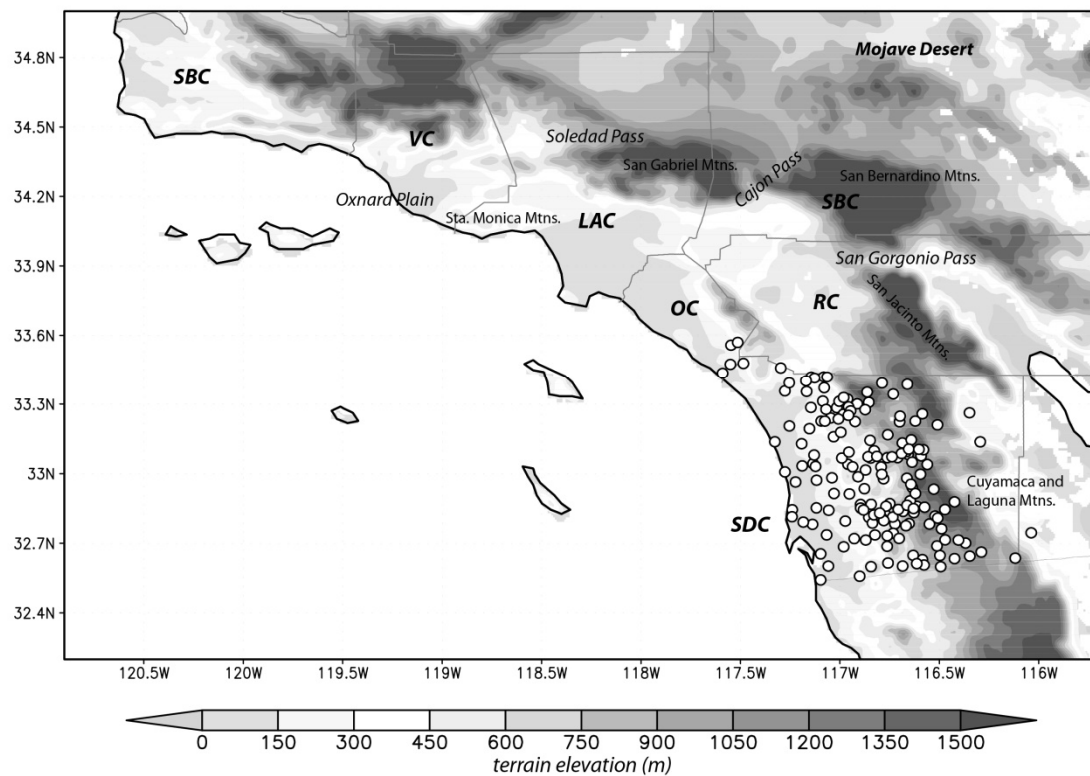

Fig. 1 Topography of Southern California (longitude on abscissa, latitude on ordinate), with selected place names. County outlines in grey; identifiers are Santa Barbara (SBC), Ventura (VC), Los Angeles (LAC), Orange (OC), San Bernardino (SBC), and Riverside (RC)

[†] This location was confirmed with San Diego Gas and Electric. The California Department of Forestry and Fire Protection report lists two different origins, one clearly erroneous and the other on Hwy 78 near Witch Creek mountain, a few km from the actual ignition site.
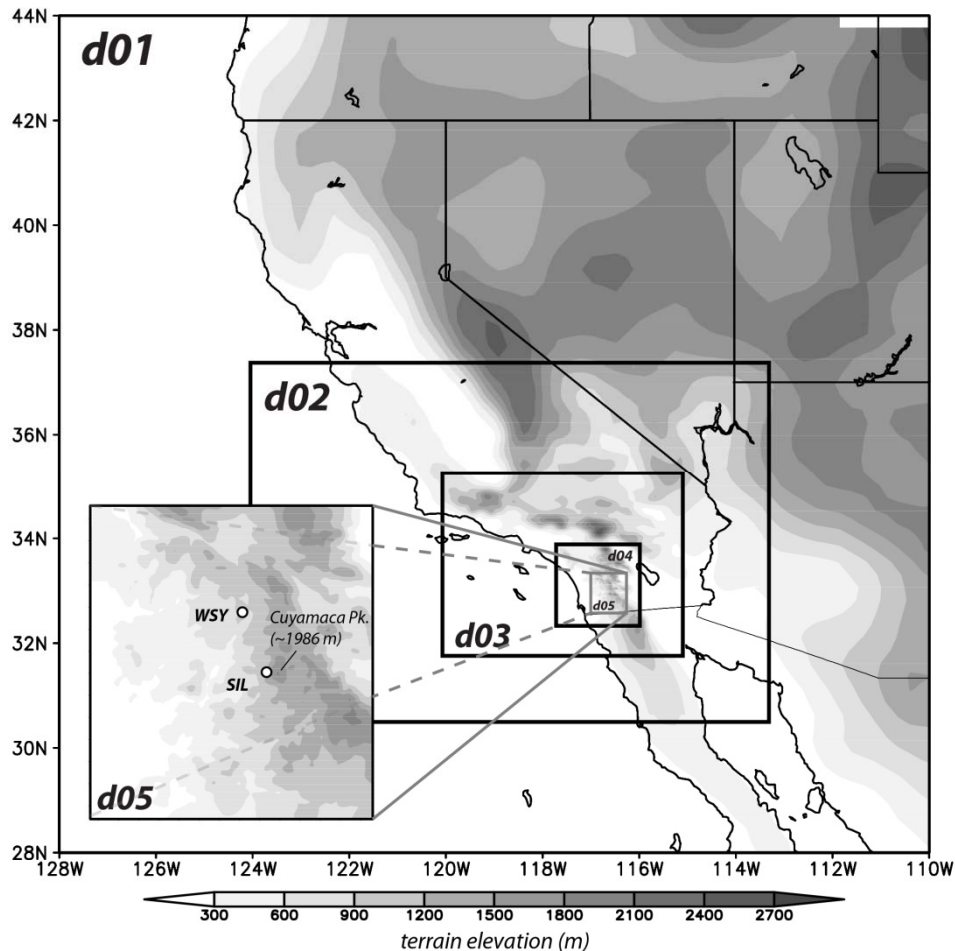
Fig. 2 Model domain configuration for the WRF-ARW simulations, with topography shaded. Domains 1-5 employ grid spacings of 54, 18, 6, 2 and 0.667 km, respectively. Locations of WSY and SIL are shown on Domain 5 inset (d05)

This study emerged from a need to estimate the event maximum wind speeds (sustained winds and gusts) at the Witch fire ignition site, a location for which no good, representative meteorological data were available. Existing stations were too far away and/or negatively influenced by obstacles such as buildings or trees (cf. Cao and Fovell 2016). Even if all observing sites were well-exposed and handled uniformly, it remains that winds are very strongly influenced by terrain, and thus can vary substantially even over rather short distances. This is where numerical modeling can help fill the spatial and temporal observational gaps, but models need to be verified and calibrated, which can be a problem when observing systems tend to vary with respect to sensor hardware, averaging, sampling and reporting intervals, and even (and perhaps especially) mounting height.

Subsequent to the 2007 firestorm, the San Diego Gas and Electric (SDG&E) company started building a high density, limited-area observational network (a "mesonet") in San Diego County, consisting of instruments installed on electrical poles at a height of 6.1 m AGL in wind-prone areas (see white dots on Fig. 1). The roughly 140 stations presently in this mesonet employ uniform hardware as well as siting and sampling strategies. We will examine the spatial and temporal structure of the October 2007 event, using model simulations verified and calibrated against SDG&E mesonet using more recent (albeit somewhat weaker) Santa Ana episodes, two of which (occurring during April and May 2014) are also investigated herein. Another such event (from February 2013) was studied in detail by Cao and Fovell (2016), which developed the experimental design used in this study. They showed that most model configurations tended to overpredict the wind, and that relatively high resolution (2 km or better) was needed to properly represent the terrain shape that helped determine the magnitude and location of the fastest downslope winds.

The structure of this paper is as follows: Section 2 provides information regarding the model simulations and observations used to verify them, and Sec. 3 provides background on two particular stations of interest in the SDG&E mesonet. Sections 4-6 focus on particular Santa Ana events, including the October 2007 windstorm, identifying potentially contributing factors to the production of intense gusts. Section 7 examines vertical wind profiles and related issues, and the summary is presented in Sec. 8.

2. Data sources and experimental design

As in Cao and Fovell (2016), version 3.5 of the Weather Research and Forecasting (WRF) model's Advanced Research WRF (ARW) core (Skamarock *et al.* 2007) was used with telescoping grids having horizontal resolutions as fine as 667 m over the complex topography of San Diego County (Fig. 2). The model was initialized using either forecast and/or analysis grids from the North American Mesoscale (NAM) model, the NCEP[‡] operational mesoscale model, or the North American Regional Reanalysis (NARR) dataset (Mesinger *et al.* 2006). NAM-based runs employed the NAM's analysis for the initial time and its 3-hourly forecasts for the outer domain's boundary tendencies, except for the October 2007 event, for which forecasts were not available, so 6-hourly analysis grids were used.   For recent events, SDG&E mesonet data were obtained from the Meteorological Assimilation Data Ingest System (MADIS) archive. SDG&E stations report sustained winds representing 10-min averages of 3-s samples, with the fastest 3-s sample in each 10-min interval representing the gust.   Simulated and observed sustained winds were compared hourly, in the manner described in Cao and Fovell (2016).

The WRF model uses a terrain-influenced coordinate system with a staggered "C" grid (Arakawa and Lamb 1977). In typical use, the WRF vertical grid is stretched, concentrating highest resolution near the surface, but with the lowest model level for scalars and the horizontal wind components ($z = Z_a$) placed at about 27 m AGL, well above the height at which the vast majority of wind observations are taken ($\leq$ 10 m). The standard practice is to assume a logarithmic wind profile between Z_a and the observation height (Z_{obs} = 6.1 m for the SDG&E network) of the form

---

[‡] National Centers for Environmental Prediction.

$$V_{obs} = V_a \frac{\ln\left(\frac{Z_{obs} - \delta}{z_0}\right) - \varphi_{obs}}{\ln\left(\frac{Z_a - \delta}{z_0}\right) - \varphi_a}, \tag{1}$$

where V_{obs} and V_a are the winds at the anemometer and lowest model levels, respectively, z_0 is the surface roughness length, δ is the so-called zero-plane displacement (typically neglected), and ψ_{obs} and ψ_a represent stability correction functions evaluated at the two heights that vanish when the surface layer is neutrally stratified, which usually occurs when the wind speeds exceed about 5 m s^{-1} (Wieringa 1976, Verkaik 2000). The roughness lengths are derived from the Moderate Resolution Imaging Spectroradiometer (MODIS) landuse database, and a United States Geological Survey (USGS) terrain database with higher resolution than the standard distributed with the WRF model is employed in San Diego County. While the assumptions inherent in the logarithmic wind profile have not been well tested in complex terrain (cf. Stensrud 2007), Cao and Fovell (2016) investigated shifting Z_a to 6.1 m, obviating the need for such assumptions, and found it not worth the extra computational expense (coming in the form of smaller model time steps) for Santa Ana wind events.

Model physical parameterizations in WRF include land surface models (LSMs), planetary boundary layer (PBL) and radiation schemes, and treatments for resolved-scale and subgrid clouds, among others, allowing an enormous number of potential configurations. Based on extensive, ~50 member model physics ensembles (Cao 2015, Cao and Fovell 2016), we have selected the Pleim-Xiu ("PX"; Pleim and Xiu 1995, Xiu and Pleim 2001) LSM and the Asymmetric Convection Model version 2 ("ACM2"; Pleim 2007) PBL options for the standard setup. This combination best represented the magnitude, spatial extent and temporal variation of the winds in the SDG&E network over a set of recent offshore wind events, including but not limited to episodes in February, October, and November 2013, and January, April, and May 2014. Most of the other physics combinations resulted in high wind biases and larger mean absolute errors with respect to the observations (Cao 2015, Cao and Fovell 2016). In many cases, that resulted from the model producing flows that remained too strong, too far down the slope.

A few caveats need to be borne in mind. Based on an extensive examination of past Santa Ana events, the October 2007 winds were very likely the strongest in San Diego County since the November 1957 episode, which means that the model was calibrated against winds that were necessarily weaker. Additionally, we only have near-surface data available for our verification, although we have been able to make logical inferences about wind patterns present farther aloft (Cao and Fovell 2016). Finally, owing to an inability to resolve subgrid scale turbulence, and relatively little spectral power at fine temporal and spatial scales, the WRF model's winds should be compared with sustained winds and not gusts (Cao and Fovell 2016).

Therefore, the properly calibrated model may still underestimate the true wind threat, which can come in the form of particularly violent wind "bursts". We will define a wind burst as a notably gusty period spanning three or more consecutive reporting intervals (i.e., 30 min), to lessen the chance that any single strong wind reading is in fact a bad observation. Starting in Sec. 4.2, gust predictions will be obtained by multiplying the sustained winds by reasonable, constant gust factors, applying a non-convective gust equation in operational use, and examining the resolved-scale winds near the surface. These estimates will be compared to available observations.

3. West Santa Ysabel and Sill Hill

Of the roughly 140 stations in the SDG&E mesonet, two are singled out for special attention: West Santa Ysabel (WSY) and Sill Hill (SIL), both being on west-facing slopes, which is the lee side during a Santa Ana episode. WSY was installed in July 2011 at 1003 m above mean sea level (MSL), approximately 0.6 km northeast of the Witch fire ignition site. This location is in a region of sparse, low-lying vegetation just downslope of a deep, narrow canyon that will be seen to be moderately well captured on the 667-m grid. Although not resolved, the ground surface also drops appreciably just to the south and southwest of the ignition location (not shown), more so than at WSY. Located 15.3 km SSE of WSY, Sill Hill has emerged as the windiest station in the network since its October 2012 installation and resides at 1084 m MSL on a steep slope west of Cuyamaca Peak (1986 m), the second highest point in San Diego County. The terrain also drops steeply immediately north of this site, which is unresolved but perhaps contributes to its especially windy conditions, and vegetation is also relatively sparse, but somewhat more dense than that in the WSY/Witch area.

Since the model cannot directly predict gusts, we need to know something about how observed gusts vary with the sustained wind. We will do this by applying reasonable gust factors (GFs), representing the ratio of the gust to the sustained wind, to the model predictions that are calibrated to remove biases. GFs can be expected to vary from site to site and time to time, reflecting specific site characteristics, vertical stability, measurement averaging periods, and also be inversely related to the sustained wind at a given location (cf., Monahan and Armendariz 1971). For the period ending 31 May 2015, there were 42230 and 33847 reports for which the sustained wind of 4 m s^{-1} or faster at WSY and SIL, respectively, the smaller count for SIL reflecting its shorter record. At both, GF variability decreased with increasing wind speed (Fig. 3), and over all observations with sustained winds ≥ 4 m s^{-1}, the average GF was 1.68 at WSY and 1.59 at SIL. At WSY, the 858 observations with sustained winds ≥ 12 m s^{-1} had an average GF of 1.59 with 99.5% of observations exceeding 1.4 and 15.0% ≥ 1.7; at much windier SIL, fully 5588 observations surpassed that threshold, with a GF average of 1.44 and all but eight samples exceeding a factor of 1.2.

However, the very strongest gusts at these sites (all occurring during Santa Ana wind events) have been associated with GFs surpassing the above-cited averages (Table 1), suggesting that higher GFs do need to be considered. At both WSY and SIL, the fastest winds were recorded on 30 April 2014, reaching 34 and 45 m s^{-1}, respectively. The WSY observation had a GF of 2.14, which represented something of an outlier during the record (Fig. 3(a)), but still would have been 2.03 had it been associated with the (larger) sustained wind reported 10 min later[§]. The other record gusts were also associated with larger than average GFs, suggesting that gust factors between 1.7 and 2.0 can occur at WSY during especially severe conditions. The SIL gusts also at least equaled that location's average GF (1.44) during windier conditions (Fig. 3(b)).

As illustrated in Fig. 4, the strongest gusts exhibit a pronounced diurnal cycle, with the highest frequencies occurring between 1500 and 1800 UTC at both locations and a secondary peak between 0500 and 0700 UTC that is more prominent at SIL. The observations employed were limited to observed gusts exceeding 20 m s^{-1} at WSY and 30 m s^{-1} at SIL, representing 826 and 741 instances, respectively. During the winter half-year, the 1500-1800 UTC interval follows sunrise,

---

[§] WSY gusts observed in the intervals immediately preceding and following this observation were both 27 m s^{-1}, representing GFs of 1.91 and 1.62.

and the other period falls in the evening before local midnight. At both locations, fast winds are rarely observed in the afternoon hours (around 0000 UTC). Although the winds were not controlled for wind direction, the substantial majority of the included observations occurred during Santa Ana events, and thus this distribution can be taken as typical of such conditions. In their case study, Cao and Fovell (2016) showed that although the February 2013 event spanned multiple days, the downslope winds were punctuated by pronounced "lull" periods that occurred around 0000 UTC (see their Fig. 6). The diurnal variation is likely tied to boundary layer evolution, which responds to diabatic surface forcing [cf. Smith and Skyllingstad (2011)].
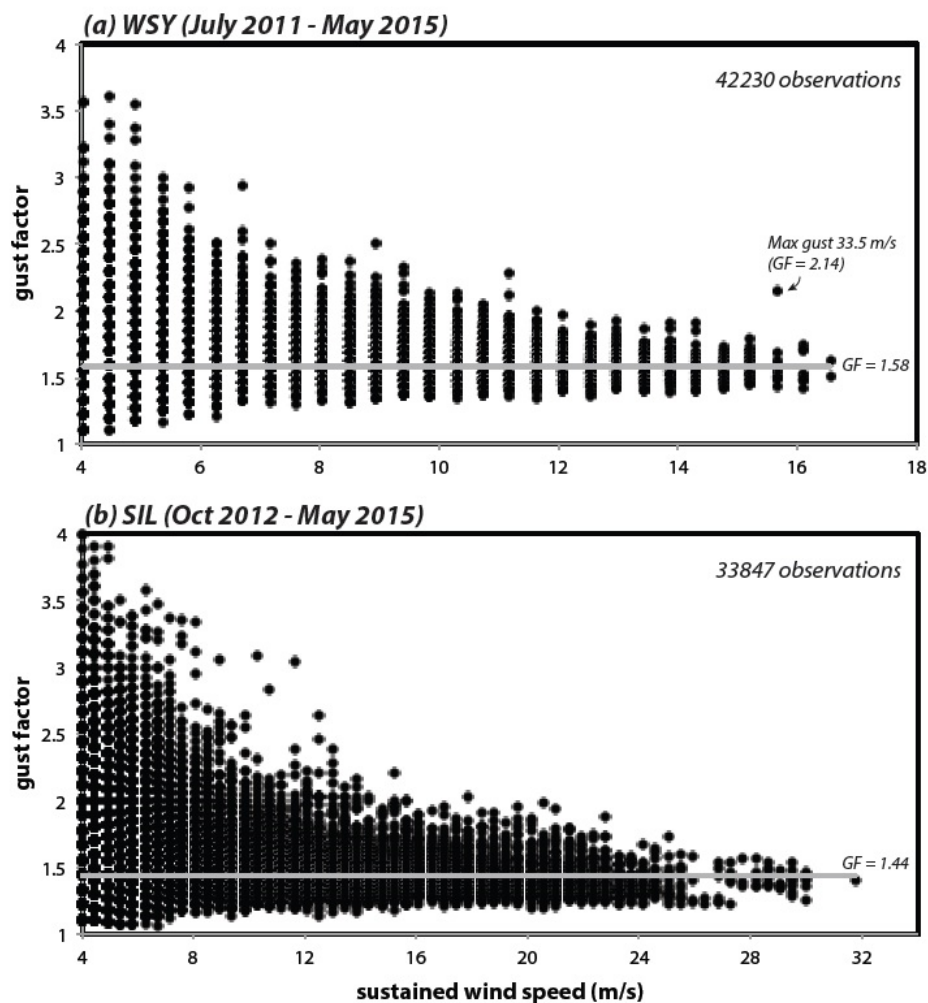

Fig. 3 Gust factors (non-dimensional) calculated from (a) 42230 observation times for the SDG&E station WSY for observations collected during July 2011-May 2015, and (b) 33847 observations times at SDG&E station SIL for observations collected during Oct 2012-May 2015, plotted against the sustained 10-min interval wind speed (m s^{-1}). Grey lines denote constant gust factors of (a) 1.58 and (b) 1.44 respectively. Note horizontal axes have different ranges
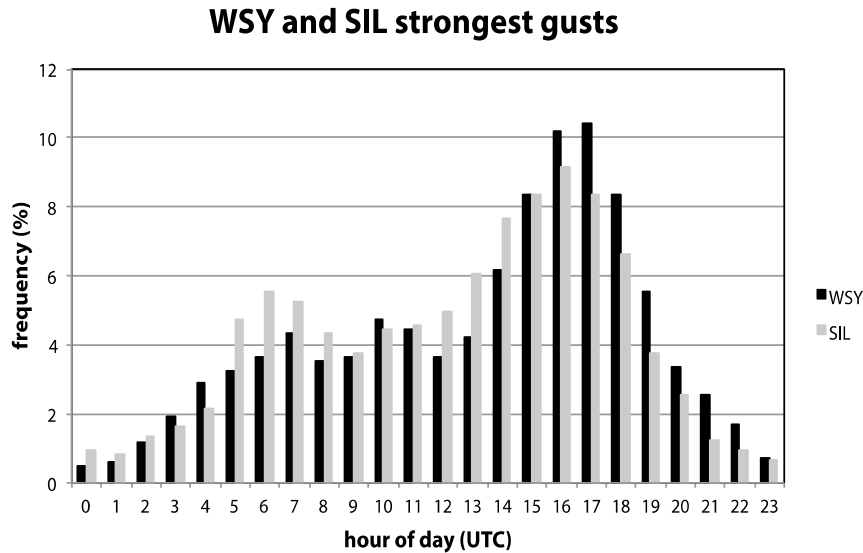
WSY and SIL strongest gusts

Fig. 4 Hourly frequency of the strongest observed wind gusts at WSY (black bars) and SIL (grey bars). Data from station installation through May 2015 were used, independent of season and wind direction, representing 826 observations ≥ 20 m s^{-1} at WSY and 741 observations ≥ 30 m s^{-1} at SIL

4. The 13-15 May 2014 Santa Ana wind event

4.1 Event evolution

Southern California has a Mediterranean type climate, consisting of hot and usually quite dry summers. As a consequence, the majority of the most destructive fires associated with Santa Ana wind events have occurred in the autumn, prior to the onset of the winter rains (Sommers 1978, Westerling *et al.* 2004). A glaring exception was the mid-May 2014 Santa Ana event, which was notable for sparking as many as 15 fires, including five exceeding 1000 acres (4 km^2) and a smaller one (the Poinsettia fire) responsible for destroying more than a dozen structures[**,††]. High temperatures and very low humidities combined with prolonged drought conditions to make the landscape more susceptible than usual to fierce downslope winds. This episode ranked second by event maximum observed gust at WSY (Table 1), and produced the 11 of the 22 fastest gust samples in this station's record. It was SIL's fifth-ranked episode, producing that station's 45th largest wind gust observation.

The May 2014 episode's network-averaged sustained winds reveal two peaks of roughly equal strength both occurring around 1700 UTC (10 AM local daylight time), about 4 hours after sunrise, separated by a pronounced lull in the early evening at 0400 UTC, about 90 min after sunset (Fig.

[**] https://en.wikipedia.org/wiki/May_2014_San_Diego_County_wildfires.

[††] http://www.carlsbadca.gov/news/displaynews.asp?NewsID=769&TargetID=1.

5). Both the magnitude and the temporal variation of the mesonet-averaged winds are well captured in the simulation, which was initialized with NAM grids at 0600 UTC on 13 May and integrated for 54 h. While the figure demonstrates that the network-averaged wind bias is nearly zero, Fig. 6(a) reveals some stations are better handled than others. As was shown in Cao and Fovell (2016), the wind bias is quite variable in space, especially in the "central area" (Fig. 6(b)). Note that while WSY is well-predicted with respect to the event-averaged wind, SIL and several other stations are dramatically underforecasted and the simulated YSA (Santa Ysabel) and PIH (Pine Hills) winds are too strong.

Somewhat similar to Cao and Fovell (2016), the May 2014 event's two phases evinced different evolutions in the vicinity of WSY (Fig. 7(a)) with respect to observed winds and gusts. During the first phase, the gusts waxed and waned nearly simultaneously at stations JUL, WSY, WCK, and SSO, which are aligned east to west along the northernmost dashed line shown in Fig. 6(b), with JUL being close to the ridgeline. Magnitudes were also comparable among those sites, although WSY's winds were more variable and more subject to relatively short-period wind bursts, as defined earlier. The wind gust observed at WSY at 1500 UTC on May 13th was the 12th fastest recorded during the station's period of record, and tied for 5th for this particular event.

Fig. 8 presents vertical cross-sections of the westerly wind component (with negative values for east-to-west flow), taken along Fig. 6(b)'s northernmost dashed line. Superposed are isentropes, being isolines of virtual potential temperature (θ_v), a property defined as

$$\theta_v = T\left(1.0 + 0.61 q_v\right)\left[\frac{p_0}{p}\right]^{R_d/c_{pd}} \tag{2}$$
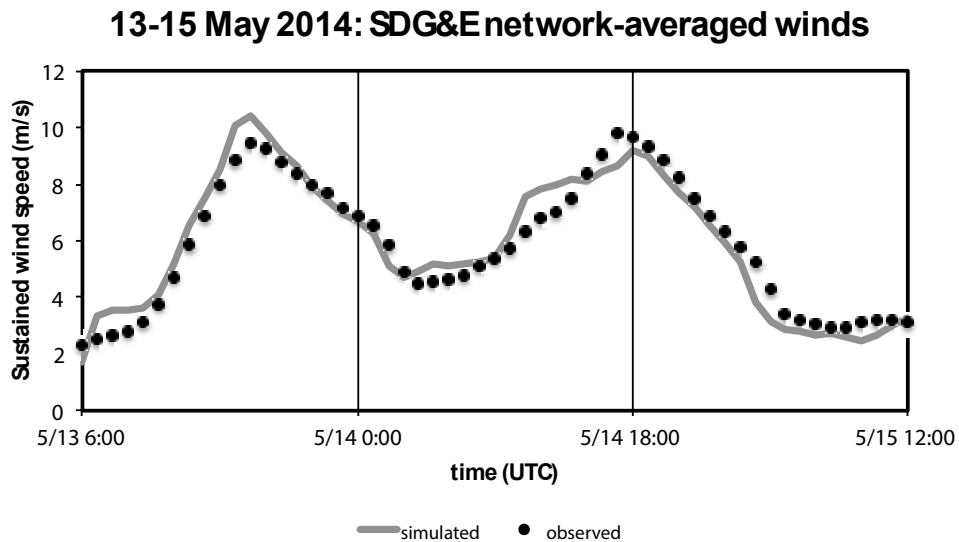
13-15 May 2014: SDG&E network-averaged winds

Fig. 5 Time series of SDG&E network-averaged sustained winds observed (black dots) and simulated (grey curve) for the 13-15 May 2014 Santa Ana wind event, based on 142 stations
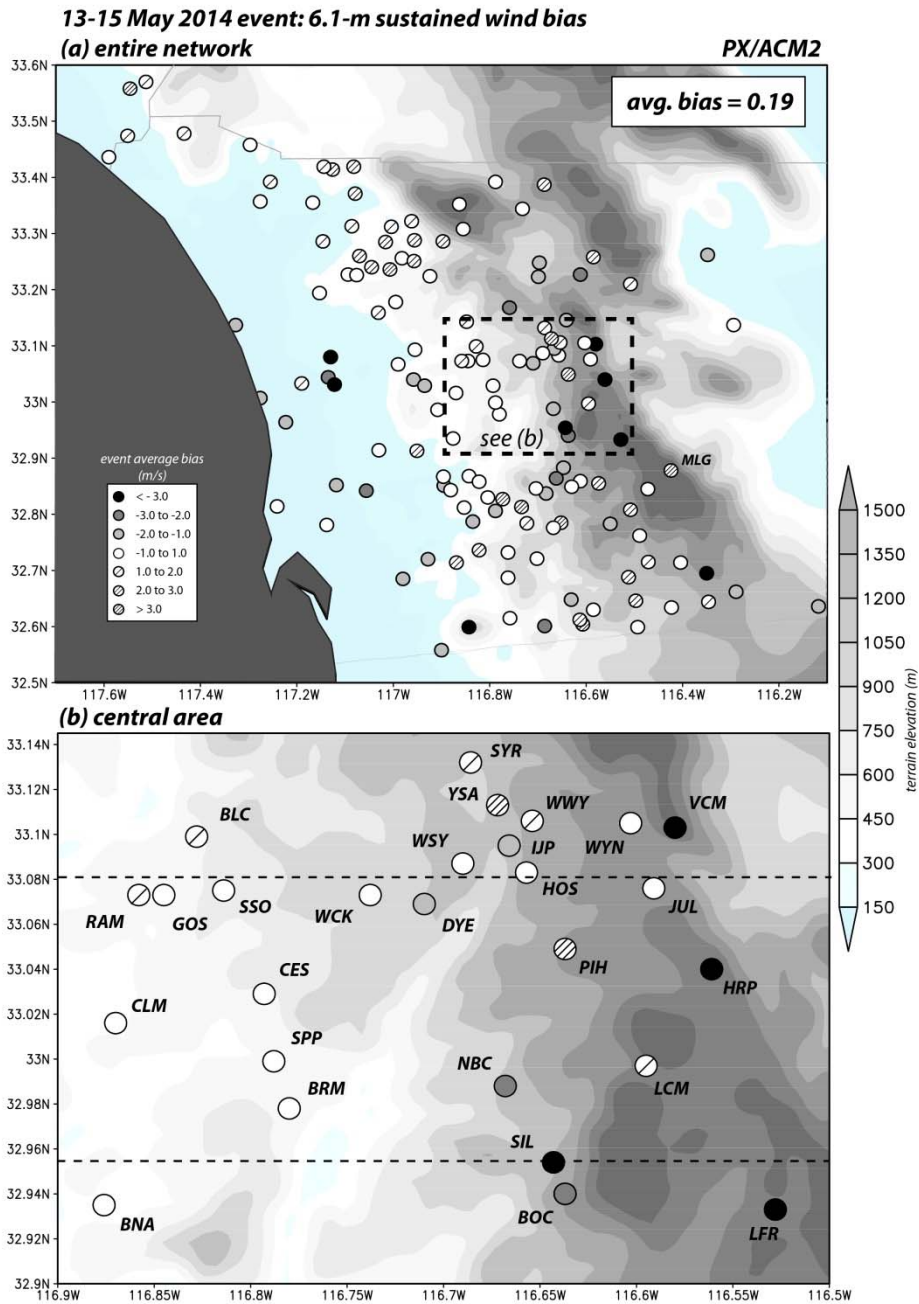
Fig. 6 Event-average wind bias relative to the observed wind for the 13-15 May 2014 Santa Ana wind event, using the control model configuration (including the PX/ACM2 physics combination) showing (a) the full SDG&E network, and (b) stations in the central area including WSY and SIL. Model topography of the 2 km domain (longitude on abscissa, latitude on ordinate) is shown as the shaded field
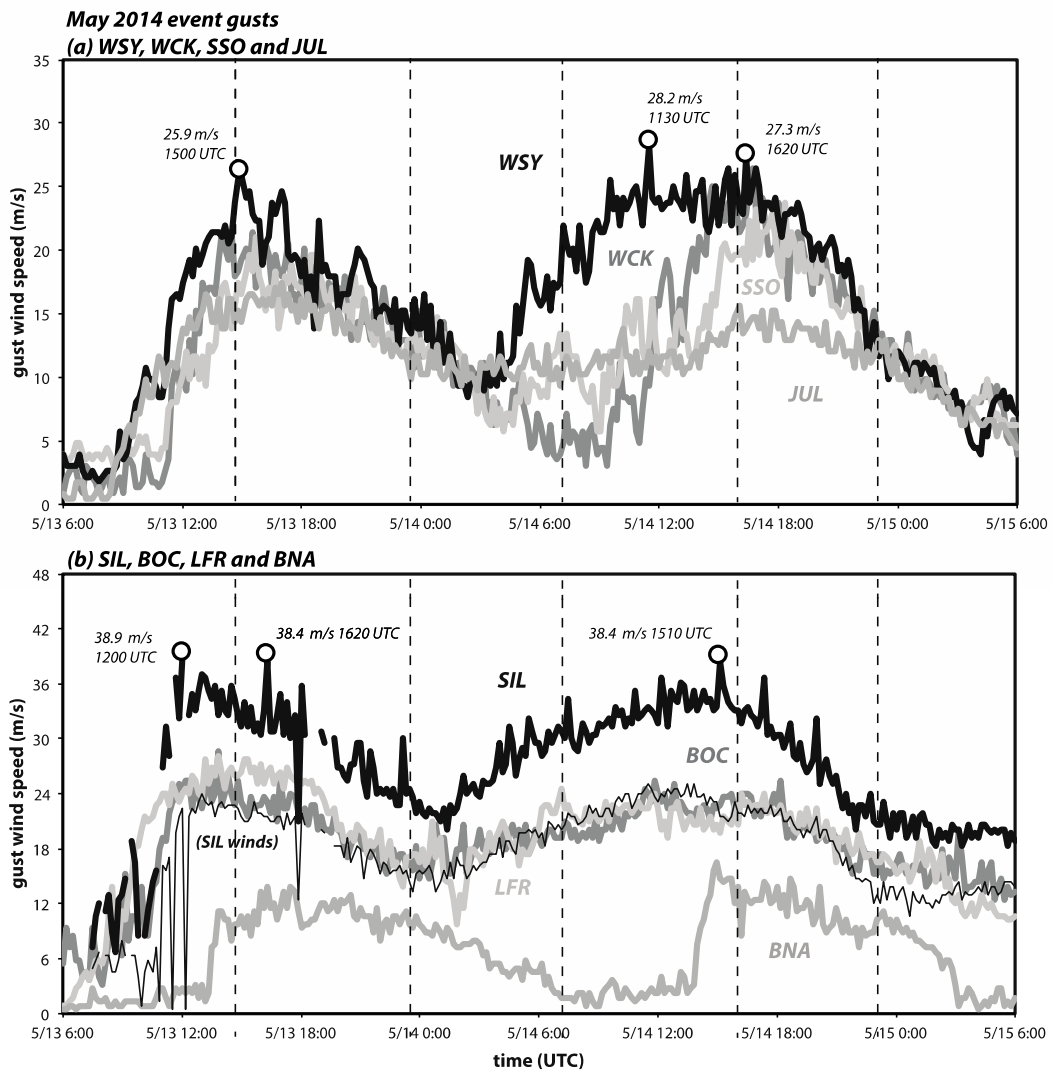
Fig. 7 Time series of observed gusts (m s⁻¹) over two days at (a) WSY, WCK, SSO and JUL; and (b) SIL, BOC, LFR and BNA. On (b), sustained winds (thin black line) for SIL are superposed. Vertical dashed lines correspond to times of Fig. 8. Some maxima are highlighted
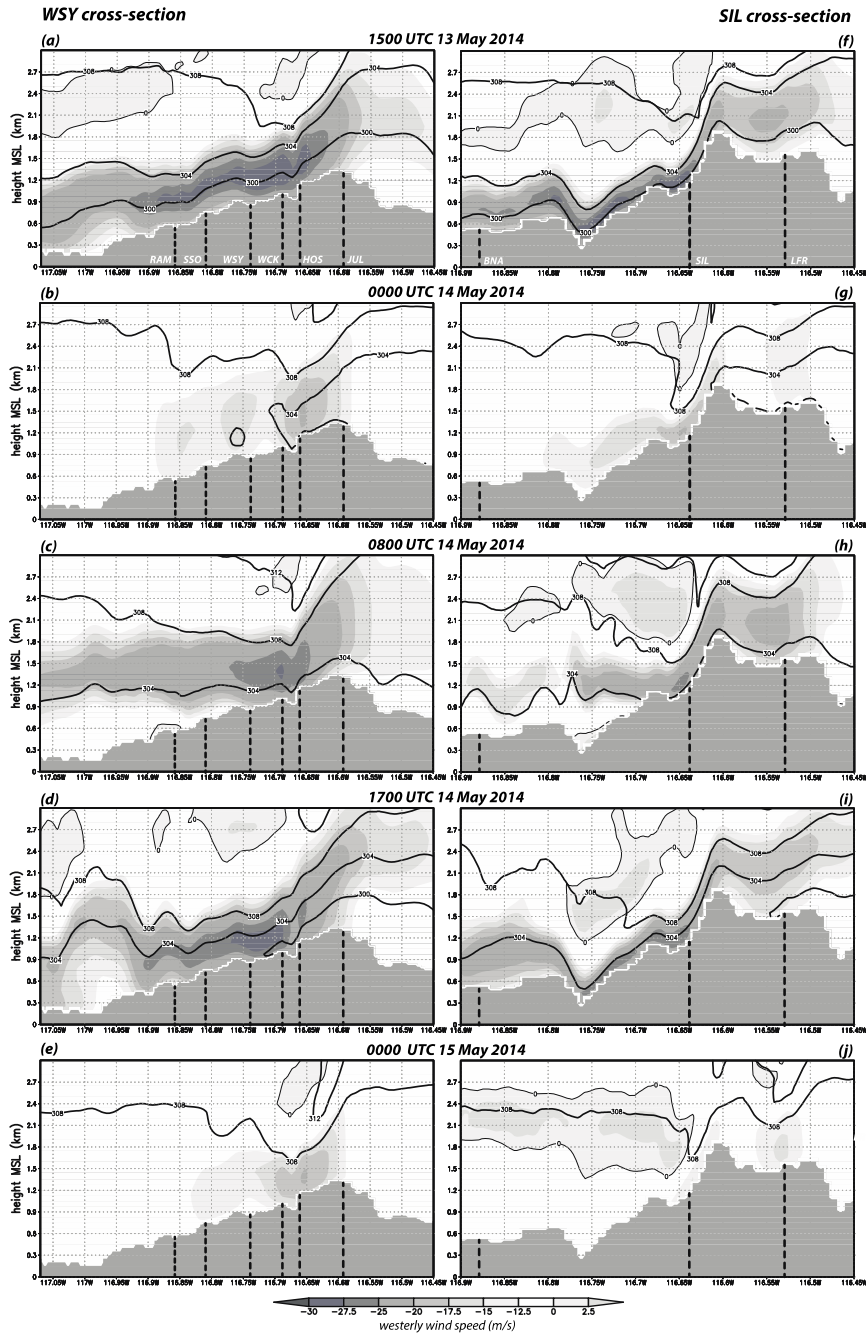
Robert G. Fovell and Yang Cao

WSY cross-section   **SIL cross-section**

Fig. 8 West-east vertical cross-sections (longitude on abscissa) of zonal wind speed (shaded, with zero thin contours) for five times during the 13-15 May 2014 event, taken west-east across (a-e) WSY and (f-j) SIL with underlying topography in grey (see Fig. 6(b)). Thick contours denote isentropes of virtual potential temperature (4 K interval). Approximate locations of some SDG&E stations are marked. Stations WCK, SSO, JUL, RAM, HOS, BNA, and LFR are displaced somewhat from the vertical plane depicted

where T is absolute temperature, q_v is the water vapor specific humidity (kg of vapor per kg of air), p is the pressure, the reference pressure p_0 is 1000 hPa, and R_d and c_{pd} are the dry air gas constant and specific heat at constant pressure, respectively. θ_v is conserved in the absence of diabatic heating and mixing, and can be used to roughly visualize flow streamlines (rather than trajectories) as well as stability (via their vertical variation). During this phase, the model produced a deep and spatially extensive layer of strong easterly winds west of the ridgeline (Fig. 8(a)). Note that westbound parcels passing over the crest are subject to considerable descent. The winds extended far along the slope before and after this time (not shown), and even reached the coastline where the Bernardo fire started (at about 1700 UTC on May 13th). In many Santa Ana wind events, the winds have lofted well above the ground by the time the flow has reached the ocean.

By 0000 UTC May 14th (Fig. 8(b)), the winds had diminished almost everywhere. The observations (Fig. 7(a)) and simulation (Figs. 8(c) and 8(d)) both suggest the second phase exhibited a clear downslope progression, as faster winds appeared earlier (i.e., the lull ending sooner) higher up on the slope. During this second phase, wind speeds remained decidedly weaker at the ridge (JUL). This is reminiscent of the second half of the February 2013 episode (Cao and Fovell 2016), and is captured in the model cross-sections. The weak flow seen at 0000 UTC May 15th (Fig. 8(e)) is not just a lull, but also the end of this roughly 2-day event.

At SIL (Fig. 7(b)), gusts exceeded 38 m s^{-1} during both phases, representing the fastest winds observed in the mesonet during this event. Like WSY, the Sill Hill site evinced frequent, short-period spikes in the reported gusts. Note that the flow at anemometer level was much weaker at BOC, only 1.6 km away and slightly farther (at 1130 m MSL) up the slope, and at LFR (11 km away, at 1445 m MSL). In fact, as occurred in the February 2013 episode, SIL's sustained winds were comparable to BOC's (also LFR's) *gusts*. There is good reason to believe that the reported winds are characteristic of the site, and the equipment is operating properly (Brian D'Agostino and Steve Vanderburg, personal communication, 2013). As SIL and BOC represent neighboring grid points on the 667 m grid (and the same point at coarser resolution), forecasts for the two sites are nearly identical, so it would be impossible to accurately simulate the winds at both sites simultaneously. The topographic feature that ostensibly helps SIL's winds to often be so much stronger than BOC's during Santa Ana wind events is not resolvable in the current experiment.

The broader-scale topography in the west-east plane crossing SIL is much steeper than it was across WSY, and the model suggests that the strong flow tended to be shallower as well as to conform more closely to the terrain during the first phase of the event (Fig. 8(f)). This characteristic places faster winds closer to the surface in the vicinity of Sill Hill. Following the lull, the simulated winds were lofted to the west of SIL as the second phase commenced (Figs. 8(g) and 8(h)), but subsequently descended to the surface again (Fig. 8(i)). This is consistent with the observations recorded at BNA, located farther down the slope (Figs. 6 and 7(b)). (Note the sudden increase in wind speeds following 1400 UTC May 14th, which falls between the times of Figs. 8(h) and 8(i)). At all times, the strongest winds tend to be found in the local terrain depression located just downslope of SIL, in an area devoid of stations. It is possible the windiest spot in San Diego County is actually just downslope from the Sill Hill site.

4.2 Inferring wind gusts from sustained wind forecasts

Accurate predictions of winds and gusts for locations in San Diego County, particularly for the Witch fire site during the October 2007 event, are essential since winds and gusts help spread fires. An important part of this exercise is model calibration, to identify and mitigate (if not eliminate)

biases from the sustained wind reconstructions. Because gusts can fluctuate so rapidly with time at some stations, as demonstrated above for WSY and SIL, we have to accept that any particular forecast may possess considerable error, but our expectation is we can learn something useful about how fast an event's maximum winds might be and when they might occur.

Fig. 9 compares simulated with observed sustained winds at WSY, SIL, and three other nearby stations for the May 2014 case. Both the magnitude and the evolution of the winds are well simulated at WSY but are significantly underpredicted at SIL. As suggested by Fig. 6(b), forecasts at stations IJP and VCM are also negatively biased while YSA is overpredicted by 100%. As with SIL, the negative biases at IJP and VCM likely represent unresolved landforms that serve to amplify the offshore wind at those sites. Station YSA is sited just west of a very steep cliff that is not rendered properly even in the 667 m domain, placing the actual site in an unresolved wind shadow.
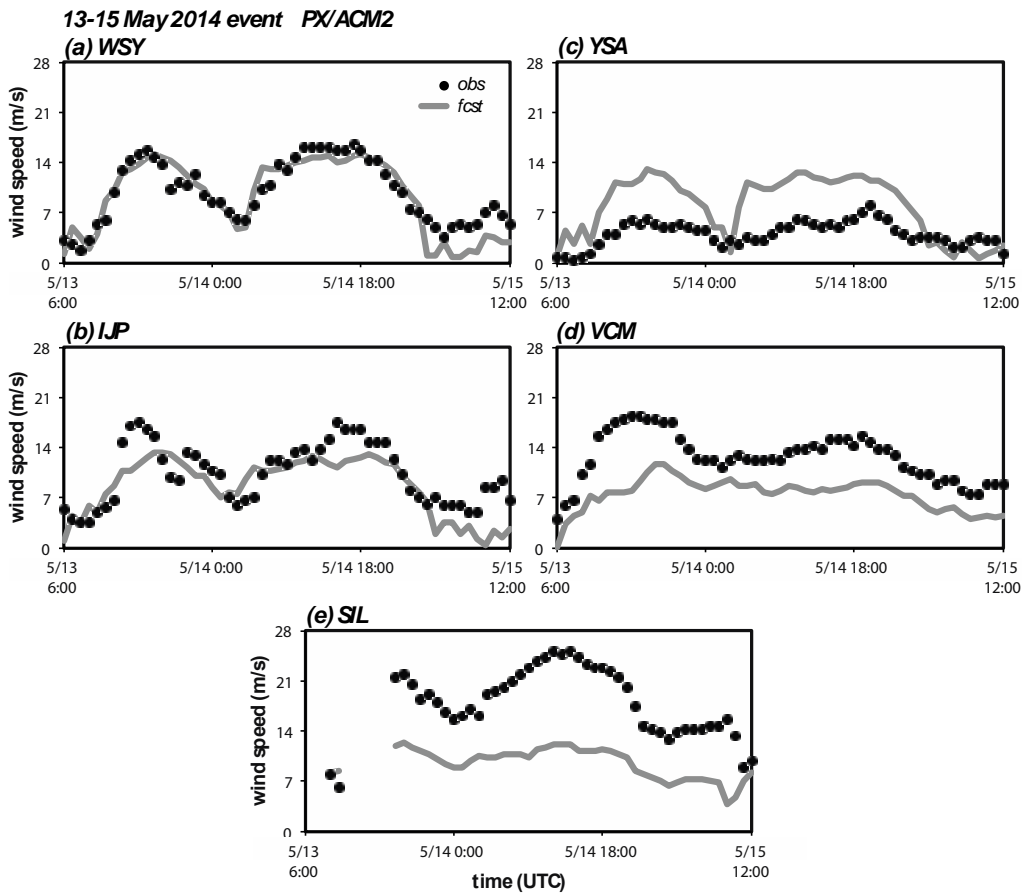

Fig. 9 Time series of observed (black dots) and predicted (grey curves) 6.1-m sustained winds (m s^{-1}) for the 13-15 May 2014 event at stations (a) WSY, (b) IJP, (c) YSA, (d) VCM, and (e) SIL
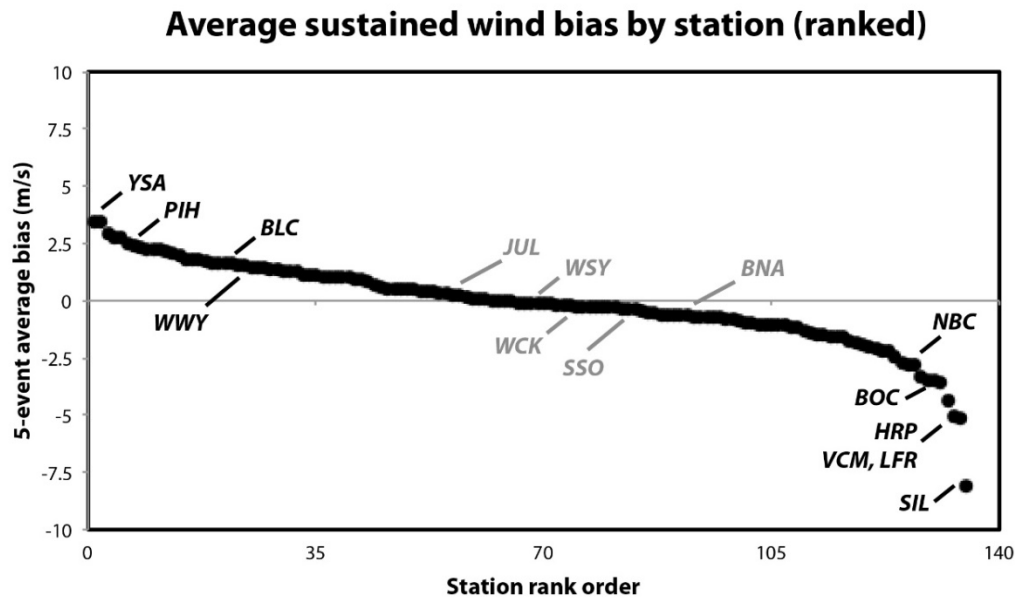
Fig. 10 Sustained wind bias, averaged over five Santa Ana events (February and October 2013, April and May 2014, and January 2015), in rank order with selected stations identified. Only the 137 stations available for all five events are included

The most poorly handled stations are quite consistent from event to event. Fig. 10 presents average event sustained wind biases aggregated over five separate episodes (February and October 2013, April and May 2014, and January 2015) for 137 stations consistently available since 2013. The distribution of errors among stations is essentially Gaussian with (as in the May 2014 case) a mean bias that is statistically indistinct from zero. YSA has second-highest positive average forecast error (3.2 m s^{-1}) among the 137 stations included in this analysis[‡‡] while SIL's is -8.4 m s^{-1}. Much of the west-facing slope is shrubland but the vegetation density around PIH is greater than in other areas and higher than suggested by the model's landuse database, likely explaining its weaker-than-predicted winds. These systematic biases most likely represent unfixable localized exposure issues and terrain features that are unresolvable on the model grid. The biases at WSY and WCK are -0.4 and -0.5 m s^{-1}, respectively, which we consider negligible.

Fig. 11 presents gust forecasts for WSY and SIL for the May 2014 Santa Ana and two other events that will be examined later. For WSY, the gust predictions were obtained by multiplying the sustained wind forecasts by 1.7, representing the average GF for all observations from this site with sustained winds exceeding 4 m s^{-1}. While Fig. 3(a) suggests a smaller multiplier might be appropriate, the 1.7 GF appears to work well. Some events are captured somewhat more faithfully than others, but the magnitude and timing of event's largest gusts are adequately identified. For SIL, the multiplier used was 1.6, again being representing the average GF for winds ≥ 4 m s^{-1}, applied to bias-corrected sustained winds (i.e., increased by 8.4 m s^{-1}). The plots suggest that underprediction remains an issue with this multiplier.

[‡‡] The largest positive bias, 3.7 m s^{-1}, is at station MLG, a ridgetop site closely surrounded by trees; see Fig. 6(a).
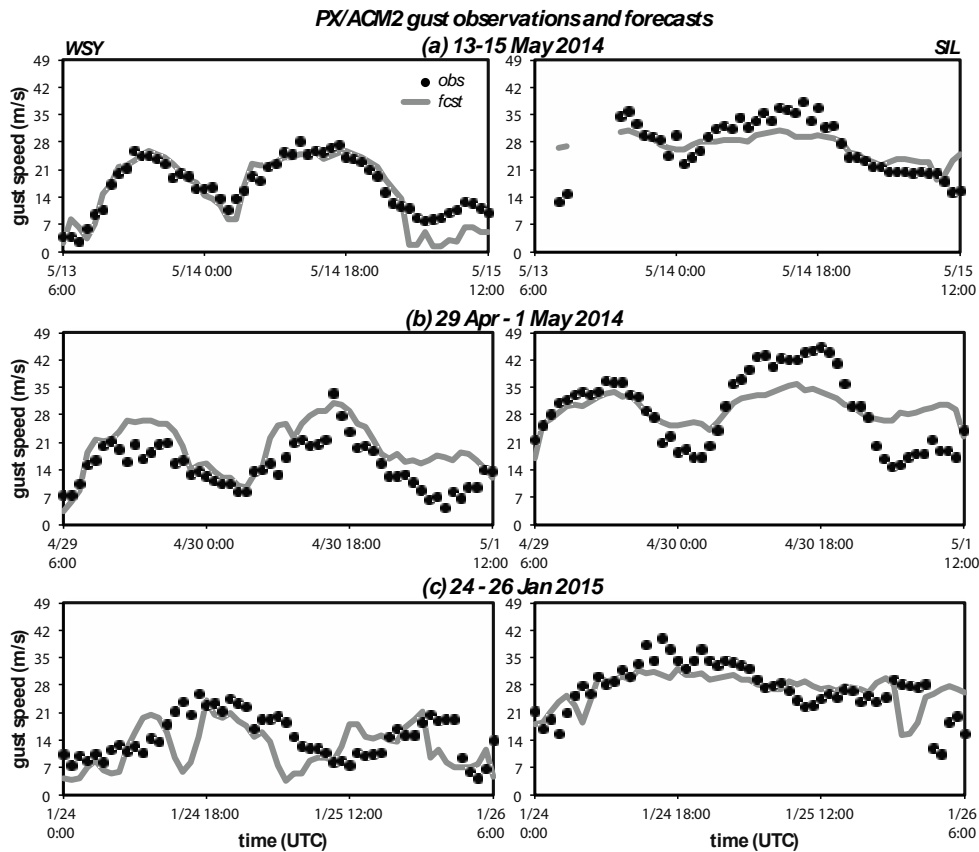
Fig. 11 Time series of observed (black dots) and predicted (grey curves) 6.1-m wind gusts (m s⁻¹) at stations WSY (left) and SIL (right) for the (a) 13-15 May 2014, (b) 29 Apr-1 May 2014, and (c) 24-26 Jan 2015 events. Gust factors used to forecast gusts are 1.7 for WSY and 1.6 for SIL respectively

5. The late-April 2014 Santa Ana wind event

The windstorm that began on 29 April 2014 yielded the fastest recorded wind and gust observations at both WSY and SIL (Table 1) during their relatively short histories. The observations (Fig. 12) reveal the episode also had two phases separated by a lull between 0000 and 0600 UTC on April 30th.   In terms of evolution, both halves of the event resembled the May 2014 episode's first phase in that the winds at WSY, JUL, WCK and SSO remained in sync and of relatively similar strength. WSY's fastest gust, 33 m s⁻¹, occurred at 1600 UTC on April 30th, during a particularly dramatic wind burst that lasted about 60 min, represented the top six gust reports for this event, and included 4 of the 7 largest values in station history. At SIL, the largest gust report was 45 m s⁻¹ for 1710 UTC on April 30, but gusts exceeded 40 m s⁻¹ repeatedly during a roughly ten-hour period stretching between 0950 and 2000 UTC. This event accounted for the top 23 gust observations at this site, and 40 of the top 44 readings, all of which surpassed 39 m s⁻¹.
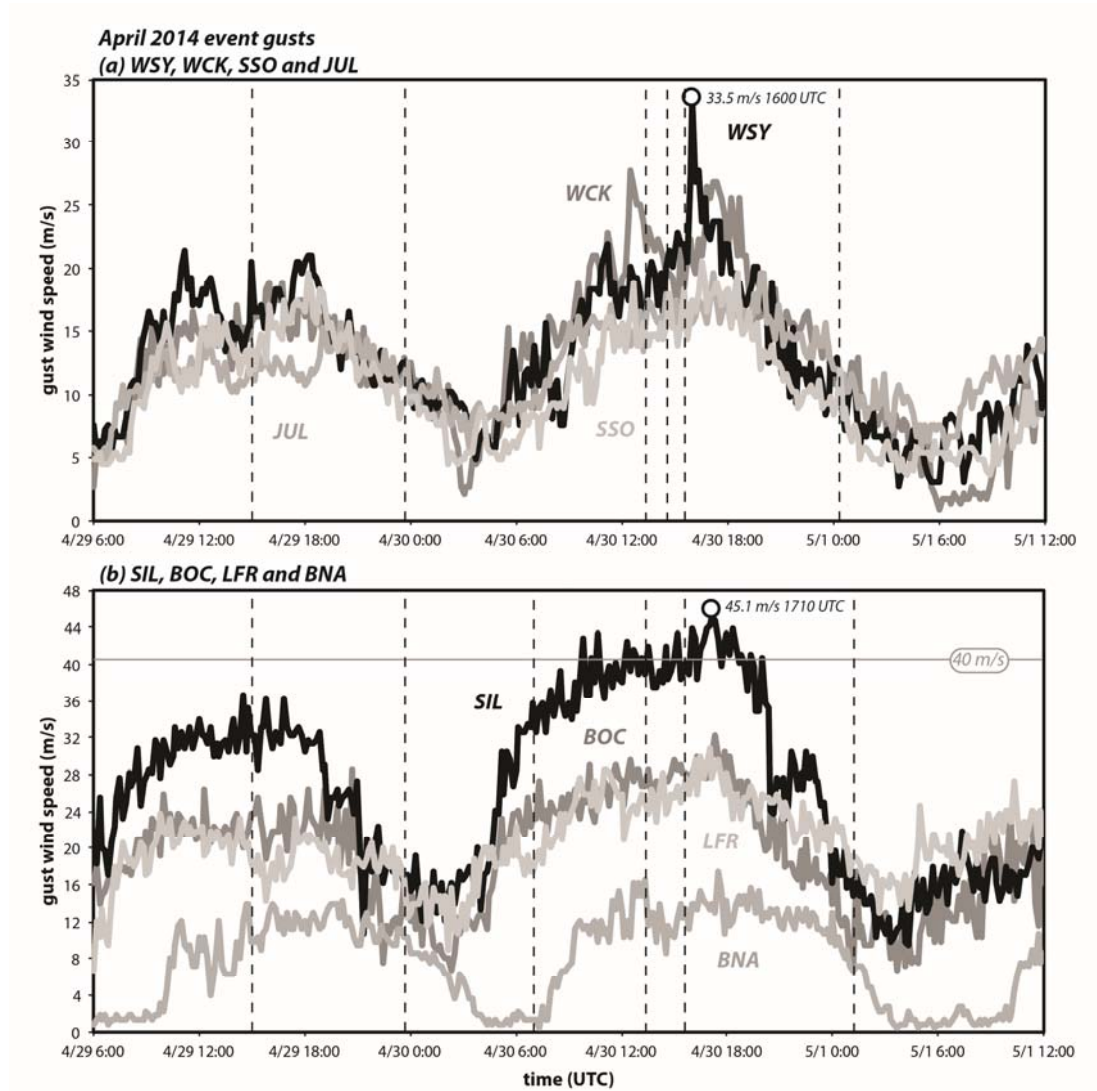
Fig. 12 Time series of observed gusts (m s^{-1}) over two days and six hours at (a) WSY, WCK, SSO and JUL; and (b) SIL, BOC, LFR and BNA. Some maxima are highlighted. Grey line denotes gust threshold of 40 m s^{-1}

The evolution of the downslope flow in the west-east cross-section including WSY is shown in Fig. 13, from a NAM-initialized simulation commencing at 0600 UTC on 29 April. The strong winds that were seen at 1500 UTC on April 29th, roughly the midpoint of the first phase, had already largely disappeared by 0000 UTC April 30th, the early part of the lull (Figs. 13(a) and 13(b)). During the peak of the second phase, an *absolutely unstable* layer develops above WSY, which is revealed by the folding of the 296 K isentrope at 1520 UTC (Fig. 13(e)) and thus represents a θ_v minimum not far above the local ground surface. In subsaturated air, absolute

instability is indicated by θ_v decreasing with height. This feature is short-lived but of interest because it might not only assist in the delivery of higher momentum air from aloft downward to the anemometer level but also help further intensify wind gusts through buoyancy-generated turbulence. At WSY, the top of the unstable layer resides at 180 m AGL, which is at or just below the level of maximum winds at this location.
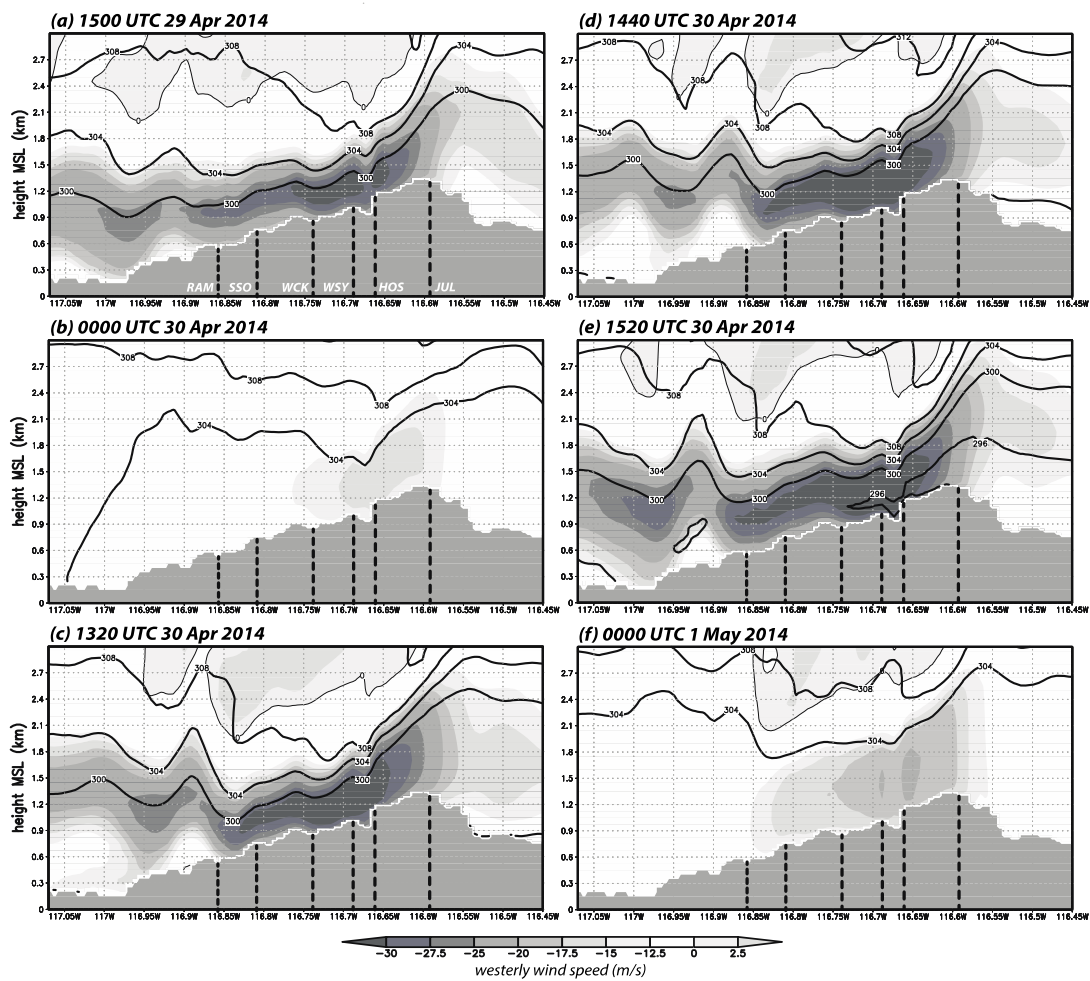

Fig. 13 West-east vertical cross-sections (longitude on abscissa) of zonal wind speed (shaded, with zero thin contours) for six times during the late April 2014 event, taken west-east across WSY with underlying topography in grey (see Fig. 6(b)). Thick contours denote isentropes of virtual potential temperature (4 K interval). Stations WCK, SSO, JUL, RAM, and HOS are displaced somewhat from the vertical plane depicted

In Fig. 14, isotherms of temperature (in ˚C) are shown along with full horizontal wind speed (dominated by the west-east component in this cross-section) for six times spanning the development of the absolutely unstable layer. Temperature is not a conserved quantity, but the isotherms help illustrate where temperature advection is occurring. Wind speeds are weak at 0400 UTC on April 30th (Fig. 14(a)), which is during the lull, and the horizontal temperature gradient across the mountain is relatively small. However, the sun had already set (by 0230 UTC) and the desert region east of the ridge cools more quickly during the evening hours, so the temperature gradient and winds both start increasing.

As the downslope flow strengthens, note the isotherms take on a concave shape above the upper portion of the lee slope (see especially Figs. 14(d) and 14(e)). This is a consequence of *differential* cold advection: the strong winds are pushing colder temperatures from the mountain's windward side down the slope, but less effectively near the surface where the winds are relatively weaker (if only owing to friction). This result is not particularly sensitive to the boundary layer parameterization employed, and occurs despite the vertical mixing it produces. As a consequence, the vertical stability in the layer extending up to the level of maximum winds is being reduced on part of the lee slope during the second episode's peak, to the point where it becomes absolutely unstable.

At favored locations, including WSY, adiabatic cooling is augmenting this destabilization; the selected isentropes (especially on Figs. 14(d) and 14(e)) show that the generally descending flow tends to follow the terrain contours. The wind impinging on the uneven terrain induces ascent above WSY (and other hills farther downslope), accounting for the temperature minimum that appears at the maximum wind level by 1600 UTC (Fig. 14(e)). That particular time is a few hours after sunrise (around 1300 UTC), and destabilization disappears as the desert side of the mountain heats up and the winds subside (Fig. 14(f)).

Fig. 15(a) presents vertical profiles of virtual potential temperature for the atmosphere above WSY before and during the development of the absolutely unstable layer. At time #① (1400 UTC), although differential cold advection has been occurring, the vertical stratification is still stable, especially very close to the surface (the model predicted temperature at 2 m AGL is depicted with circles). However, this time is about an hour after sunrise and solar insolation is increasing the surface temperature even as continued cold advection causes the 180 m temperature to fall markedly. Over the next 40 min (to time #②), the vertical lapse rate of the 0-180 m layer becomes absolutely unstable and the instability continues to increase as temperatures at the layer top do not reach minimum until between 1500 and 1600 UTC (the time of Fig. 14(e)). We note that in the observations, the largest gusts and GFs were recorded around this time.

While absolute instability in a shallow layer very close to the surface is common in boundary layers heated from below (especially later in the day), and occurs at other locations around this time, the destabilization in the vicinity of WSY represents particularly effective differential cold advection. The isochrones in Fig. 16 demonstrate the penetration of potentially cold air at 180 m AGL from the desert side through a terrain gap between Volcan Mountain and North Peak between 1436 and 1500 UTC, and arriving at WSY by 1454 UTC, using θ_v values motivated by Fig. 15. During this period, solar insolation is causing temperatures closer to the surface to rise (Fig. 15(a)), thereby decreasing the vertical stability, most dramatically where the 180 m AGL virtual potential temperature is lowest. As the wind speed remains strong through this period (see Figs. 14(d) and 14(e)), we believe that this could enhance the likelihood of strong winds and gusts occurring in this locality, which might appear in the station record associated with atypically large gust factors, as those tend to be higher under unstable conditions (e.g., Suomi *et al*. 2013).
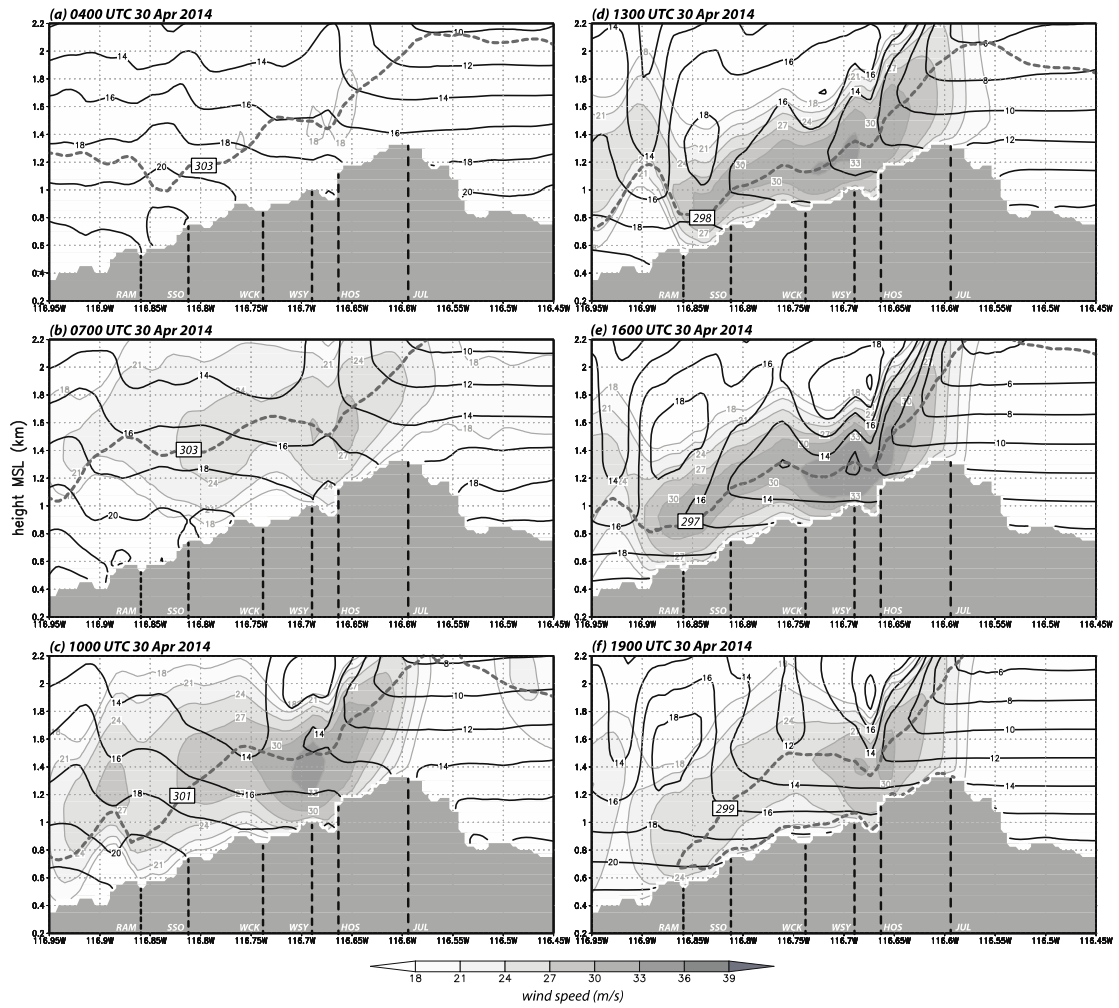
Fig. 14 West-east vertical cross-sections (longitude on abscissa) of full horizontal wind speed for six times during the late April 2014 event (shaded, with 3 m s^{-1} interval grey contours), taken west-east across WSY with underlying topography in grey (see Fig. 6(b)). Black contours denote isotherms of temperature (2˚C interval). Grey dotted contours denote isentropes of virtual potential temperature. Approximate locations of stations JUL, HOS, WSY, WCK, SSO, and RAM are marked. WCK, SSO, JUL, RAM, and HOS are displaced somewhat from the vertical plane depicted
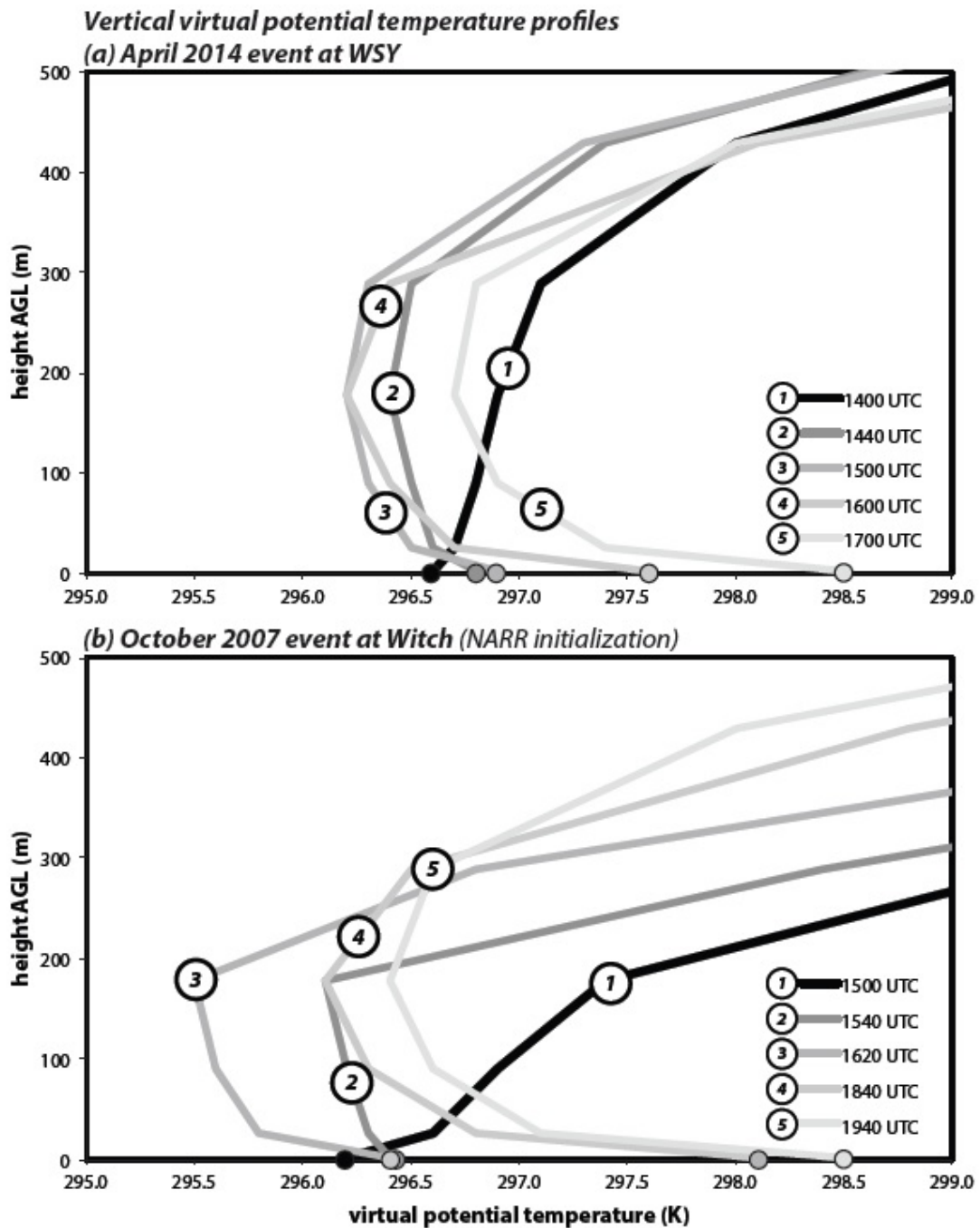
Fig. 15 Vertical profiles over the lowest 500 m AGL of virtual potential temperature for five times (a) above WSY for the April 2014 event and (b) above the Witch ignition site for the October 2007 event. Circles on the horizontal axes represent predictions at 2-m AGL
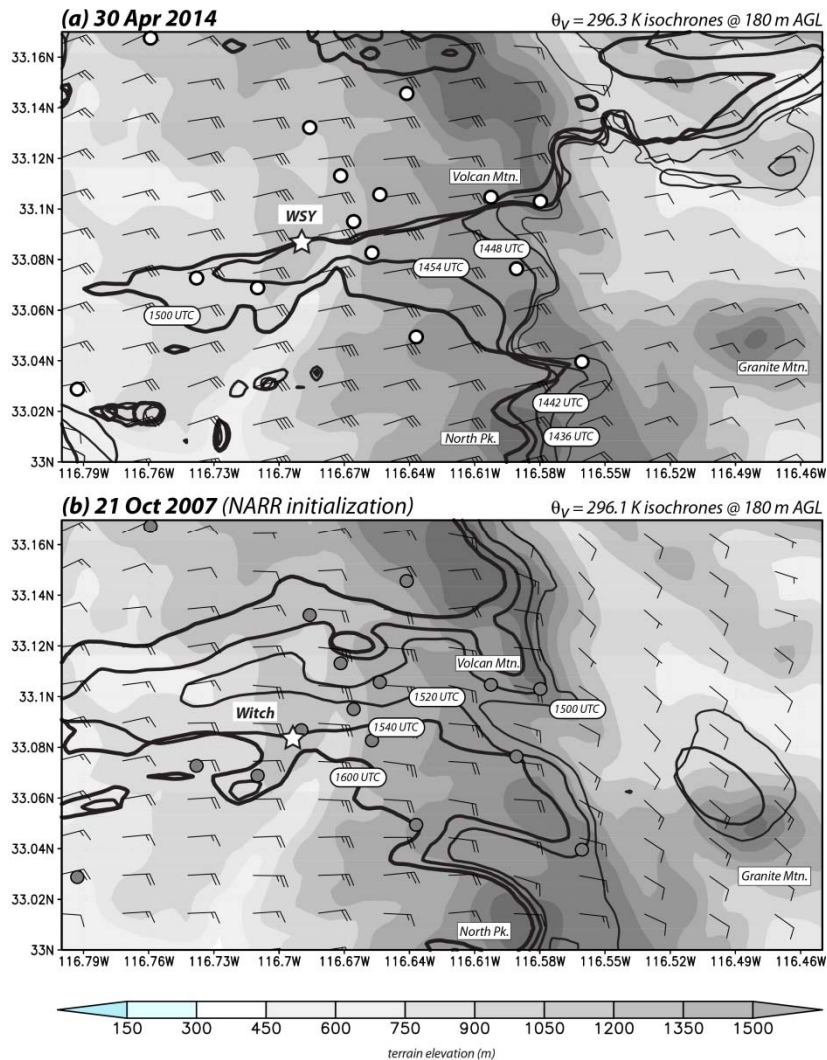
Fig. 16 Isochrones of (a) 296.3 K virtual potential temperature for the 30 April 2014 event, and (b) 296.1 K virtual potential temperature for the 21 October 2007 event, both at 180 m AGL, with topography shaded. Location of WSY on (a) is indicated with a star, and other SDG&E sites with white circles. On (b), the Witch ignition site is indicated with a star, and locations of subsequently installed SDG&E stations with grey circles are shown for reference. Simulated winds at 180 m also shown, with full and half barbs representing 10 and 5 m s^{-1}, respectively

Fig. 17 illustrates how the downslope flow evolves in the west-east plane crossing Sill Hill. As in the May 2014 case, the flow can be intense but often remains shallow, following the terrain closely, particularly in the vicinity of SIL. Panels (c)-(e) sample the extended period of very strong winds and gusts notes earlier (Fig. 12(b)). Again, we believe that part of the reason why sustained winds are so much higher at SIL is that the terrain shape helps bring the strongest winds closer to the surface than occurs at other locations, such as WSY.
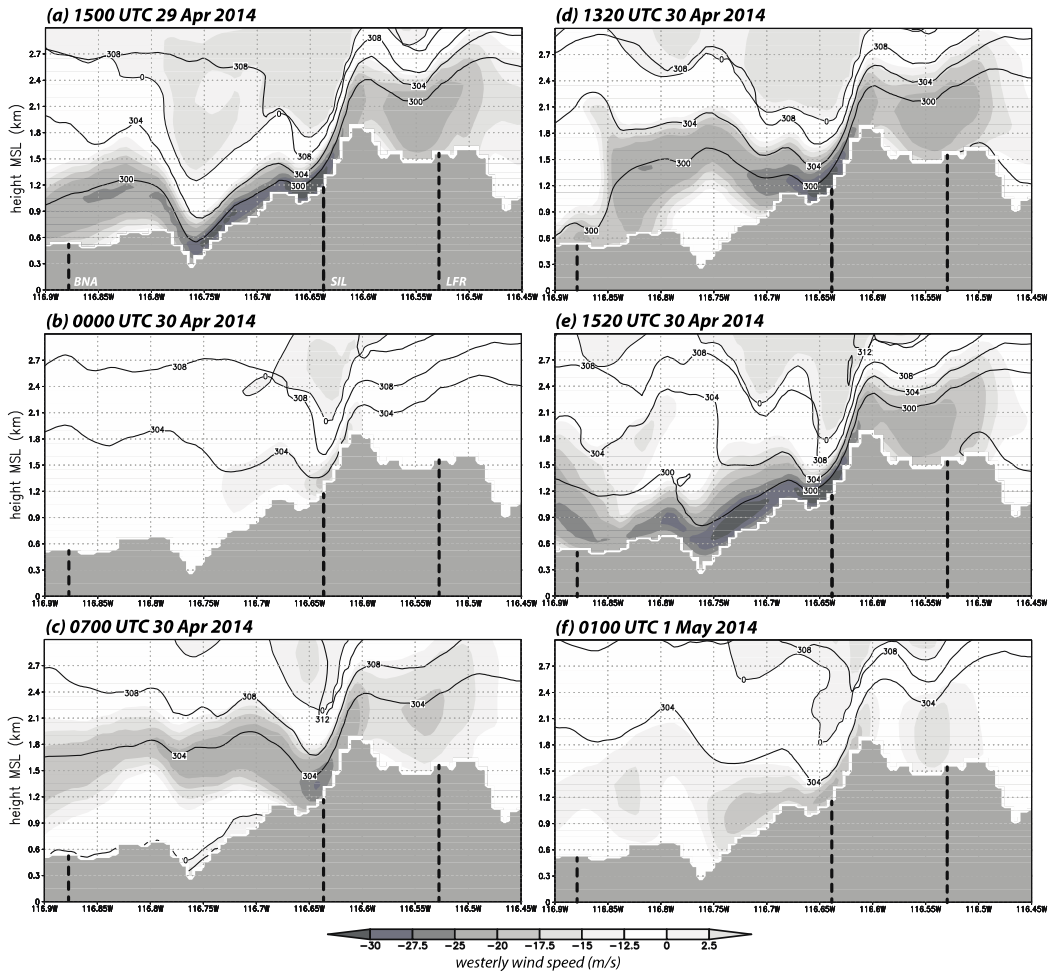
Fig. 17 Similar to Fig. 13, but for the west-east vertical plane across station SIL

6. The October 2007 Santa Ana wind event

As noted earlier, the October 2007 Santa Ana sparked and spread numerous wildfires in Southern California, including the Witch fire that started 0.6 km from subsequently-installed station WSY. In this section, we will examine two simulations of the episode, configured as described for the two 2014 cases discussed above but initiated with different data sources. One (the NAM initialization) employed the analysis and forecast grids produced by the operational NCEP model in real time. That is consistent with the manner in which the other events were initialized, but it should be borne in mind that the operational model changed significantly between 2007 and 2014. The other utilized the NARR reanalysis. Both simulations were started at 0000 UTC on October 21st.
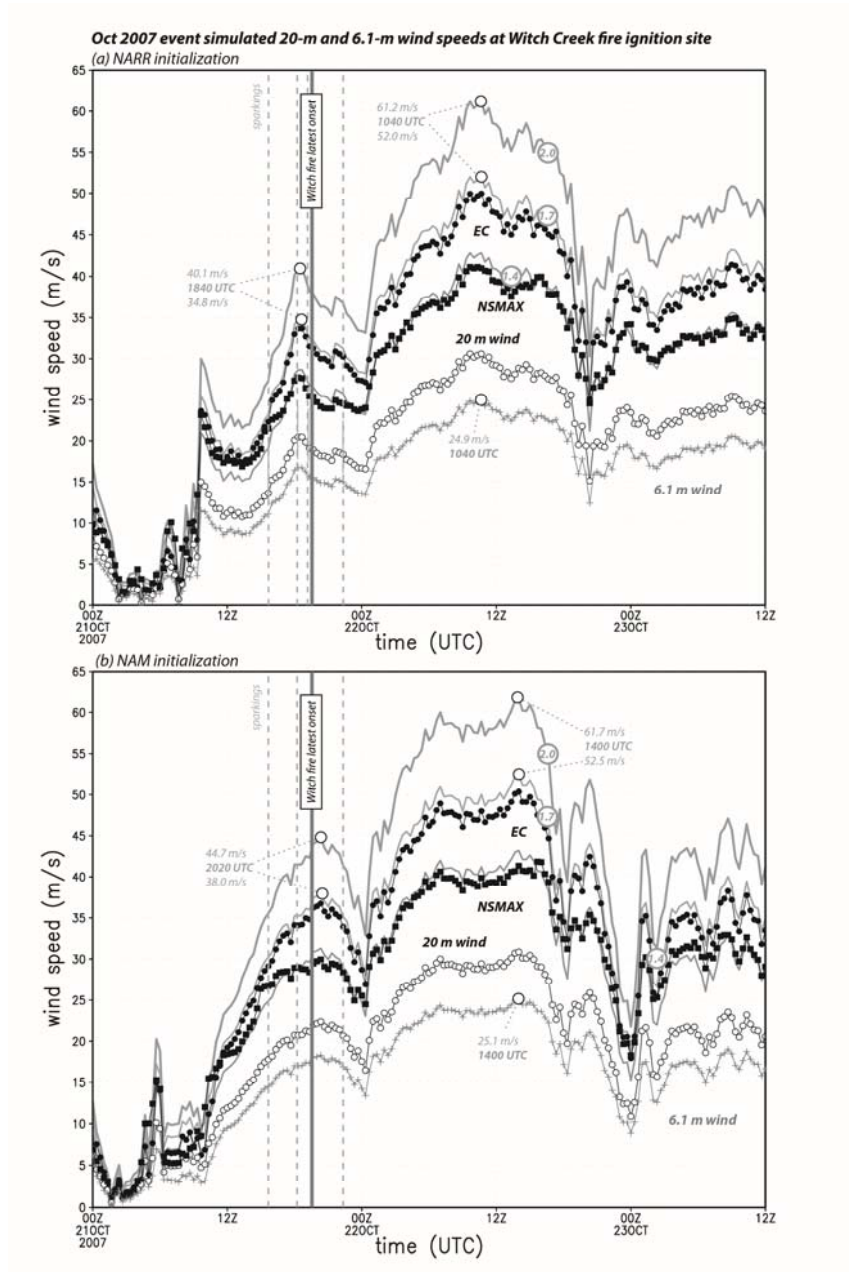
Fig. 18 Time series of 20-m and 6.1-m sustained winds and 20-m estimated gusts (m s^{-1}) employing the EC, NSMAX, and 1.4, 1.7 and 2.0 gust factor metrics at the Witch ignition site over 2.5 days from simulations made with the (a) NARR and (b) NAM initializations. Some maxima highlighted. Vertical grey dashed lines indicate reported power line sparking times, and vertical grey solid line represents the Witch fire latest onset time. Data plotted at 20 min intervals

Although they disagree somewhat with respect to intensity and timing, both October 2007 simulations generate an extremely strong Santa Ana wind event, at its peak far more intense than the April 2014 episode. Peak 6.1-m winds at the Witch ignition site were 25 m s^{-1} in both (Fig. 18), occurring between 1040 and 1400 UTC on October 22nd, significantly exceeding the largest observation in the WSY record (16.5 m s^{-1}; see Table 1). Of particular relevance are the winds at power line height, 20 m AGL, again obtained using Eq. (1). The first significant wind maximum occured around 1800-1900 UTC on October 21st, which coincided with incidents of reported power line sparking or faulting (indicated by the vertical dashed lines). The onset time of the Witch fire is not precisely known, but it must be before 1929 UTC October 21st, as a witness reported the flames at that time.

Also shown on Fig. 18 are three 20-m gust estimates made using gust factors derived from the WSY observations. As discussed earlier, GFs of 1.4 and 1.7 were exceeded by 99.5 and 15% of all reports at WSY with sustained winds $\geq$ 12 m s^{-1}, and the 2.0 factor represents exceptional bursts, as was observed during the April 2014 event (cf. Table 1) when the simulated near-surface layer was absolutely unstable (Fig. 15(a)). For WSY, the 1.7 factor appeared reasonable with respect to both the observations (Fig. 3(a)) and the reconstructions (Fig. 11), given the model's lack of bias there. One complicating issue is that GFs could be anticipated to decrease somewhat with height (e.g., Deacon 1955, Monahan and Armendariz 1971, Suomi *et al.* 2013), although it is not clear that would also occur in highly sheared, mountain-driven windstorms. Indeed, there are also reasons to believe that the 1.7 and even 2.0 GF estimates might be too *low* because the model sustained winds could be negatively biased for the Witch fire site. The SIL-BOC comparison illustrates that the wind can differ substantially during a windstorm at two neighboring, well-exposed sites and recall that the Witch fire site is close to a locally steep but to the model unresolvable drop in terrain, and thus in that respect resembles the Sill Hill landscape.

With respect to the 1.7 GF estimate, the simulations suggest that 20-m gusts on the order of 35-38 m s^{-1} could have been expected around the Witch fire onset time, leading up to event-maximum gusts of about 53 m s^{-1}. If the 2.0 GF estimate is justifiable, gusts of 40-45 m s^{-1} could have occurred during the sparking period. During that time, and in a similar manner as for the April 2014 event, an absolutely unstable layer *did* form over the site, as demonstrated in Fig. 19 for the two simulations at their respective times of maximum winds above Witch/WSY. Focusing for convenience on the NARR-based simulation, note that at 1500 UTC (profile #①) in Fig. 15(b)), 63 min after sunrise, the atmosphere above the Witch site was still stable, but absolute instability in the 0-180 m layer was already present by 1540 UTC (profile #②). The first power line fault was reported shortly thereafter (at 1553 UTC). Temperatures at the top of this layer reached minimum around 1620 UTC (profile #③), but the instability persisted past the sparking period's wind maximum for this simulation (1840 UTC, profile #④) and even the latest onset time for the Witch fire (1940 UTC, profile #⑤). As in the April 2014 case, this instability was exacerbated by the opportunistic intrusion of a potentially cold airmass from the desert over the Witch/WSY area after the sun was already heating the surface beneath (Fig. 16(b)).

While they generated relatively comparable winds over the Witch fire site, differing modestly with respect to timing and intensity, the two simulations yielded markedly different flow patterns farther downslope through the event maximum on October 22nd (Fig. 20). One run continued to push fast near-surface winds well down the slope, while the other had shifted to more of a lee-wave and/or hydraulic jump behavior in which the strongest winds were lofted. It is appreciated that downslope windstorms can be very sensitive to small shifts in conditions on the upwind side (cf., Durran 1986, Vosper 2004) and Cao and Fovell (2013) and Cao (2015) have

demonstrated that in some cases even the infusion of random noise mimicking turbulent perturbations can provoke decidedly different flow structures. During the 2007 event, there were no good observations near the Witch ignition site and, taken together, the results in this study highlight the daunting challenge of inferring wind speeds at specific sites from even high-quality data recorded upwind and farther downwind.

Two additional gust predictions labeled "EC" and "NSMAX" are provided on Fig. 18, the former utilizing the equation for non-convective gusts[§§] employed by the European Centre for Medium-range Weather Forecasts (ECMWF)

$$V_{gust} \approx V_s + 7.71u_* \tag{3}$$

in which V_s is the sustained wind speed and u_* is the friction velocity. This formula was likely developed for the standard anemometer level (10 m AGL) and may not be as applicable farther above the surface. NSMAX (for near-surface maximum) is simply the largest resolved wind speed in the lowest 180 m (the unstable layer top as is shown in Fig. 15), based on the assumption this wind could be transported downward to the height of interest by subgrid turbulence [a simple version of Brasseur (2001)]. At the Witch site, the EC gust tracks the reasonable 1.7 GF estimate closely, while NSMAX essentially represents a gust factor of 1.4 so we consider it likely to underpredict the peak winds at that and possibly other locations.
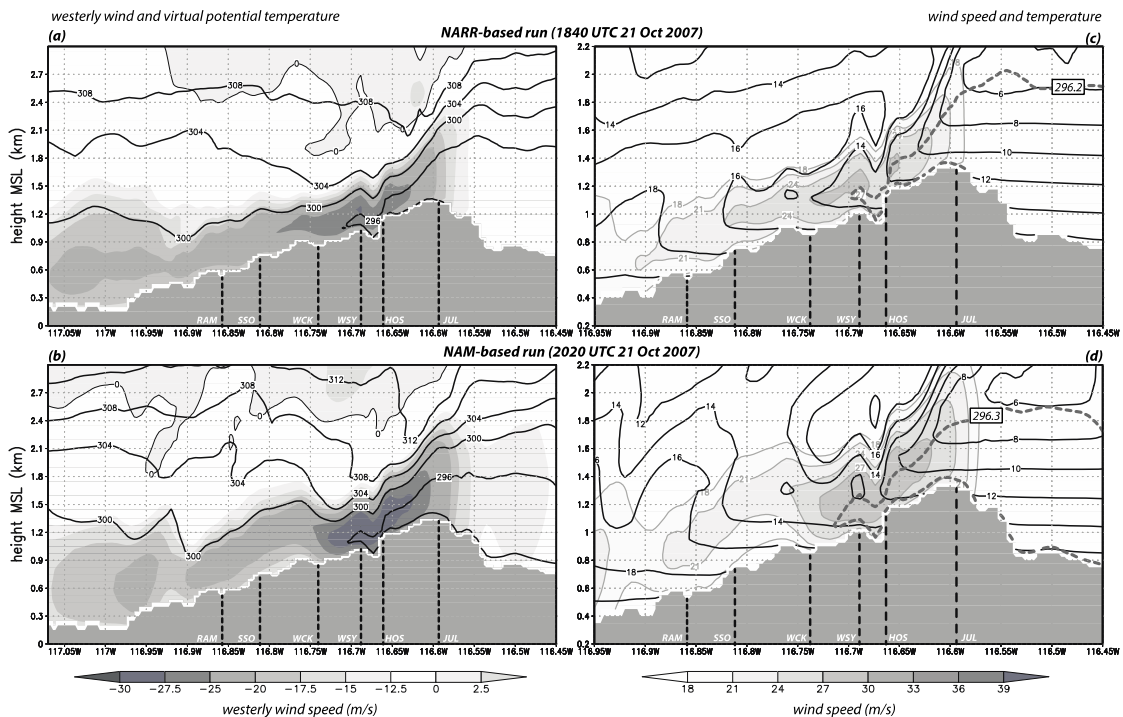

Fig. 19 Similar to Figs. 13 and 14 but for the NARR-initialized and NAM-initialized runs at their respective times of maximum winds at WSY during the sparking period on 21 October 2007
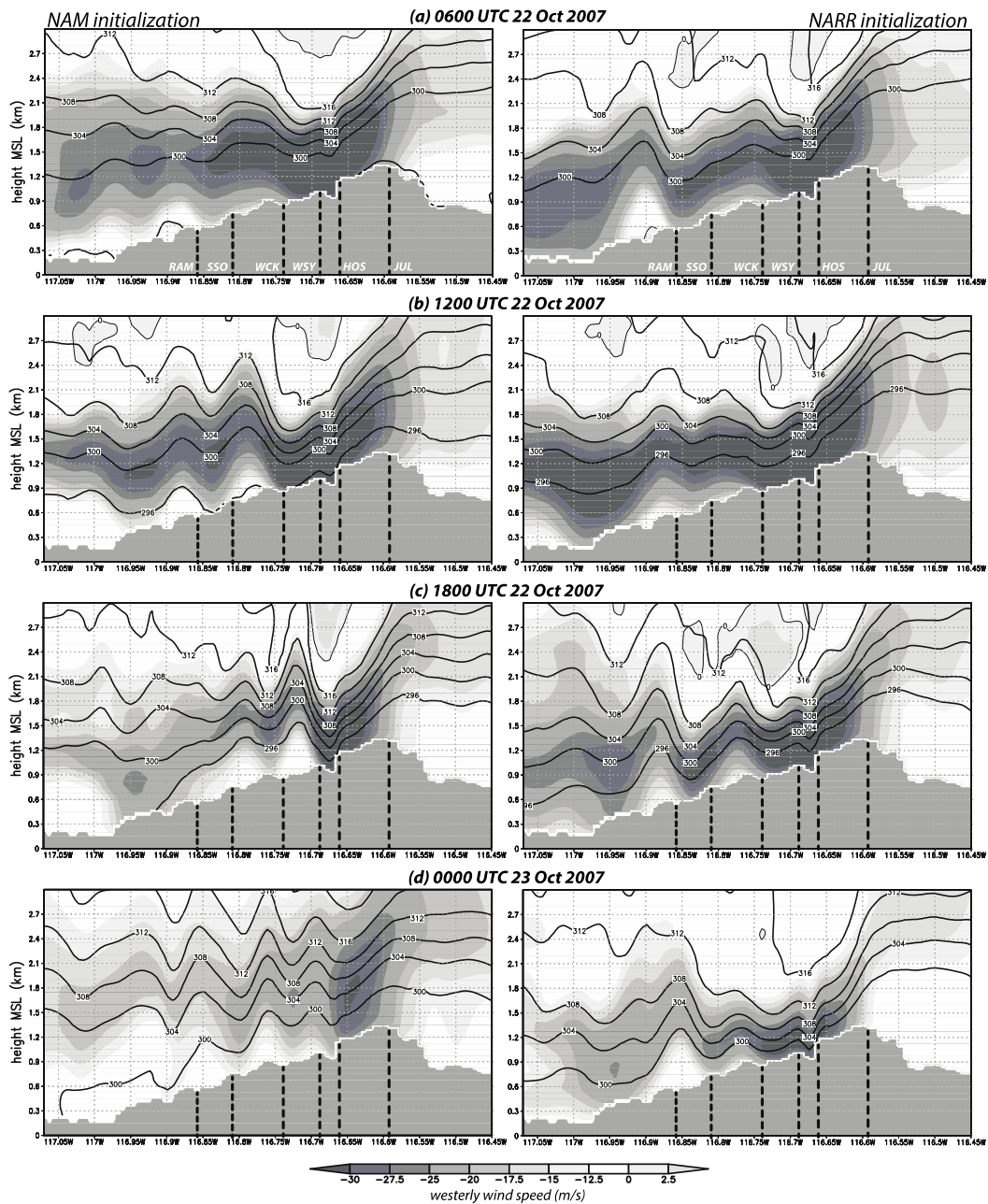
Fig. 20 Similar to Fig. 13, but for four times spanning the peak of the October 2007 event with runs initialized with NAM (left) and NARR (right)
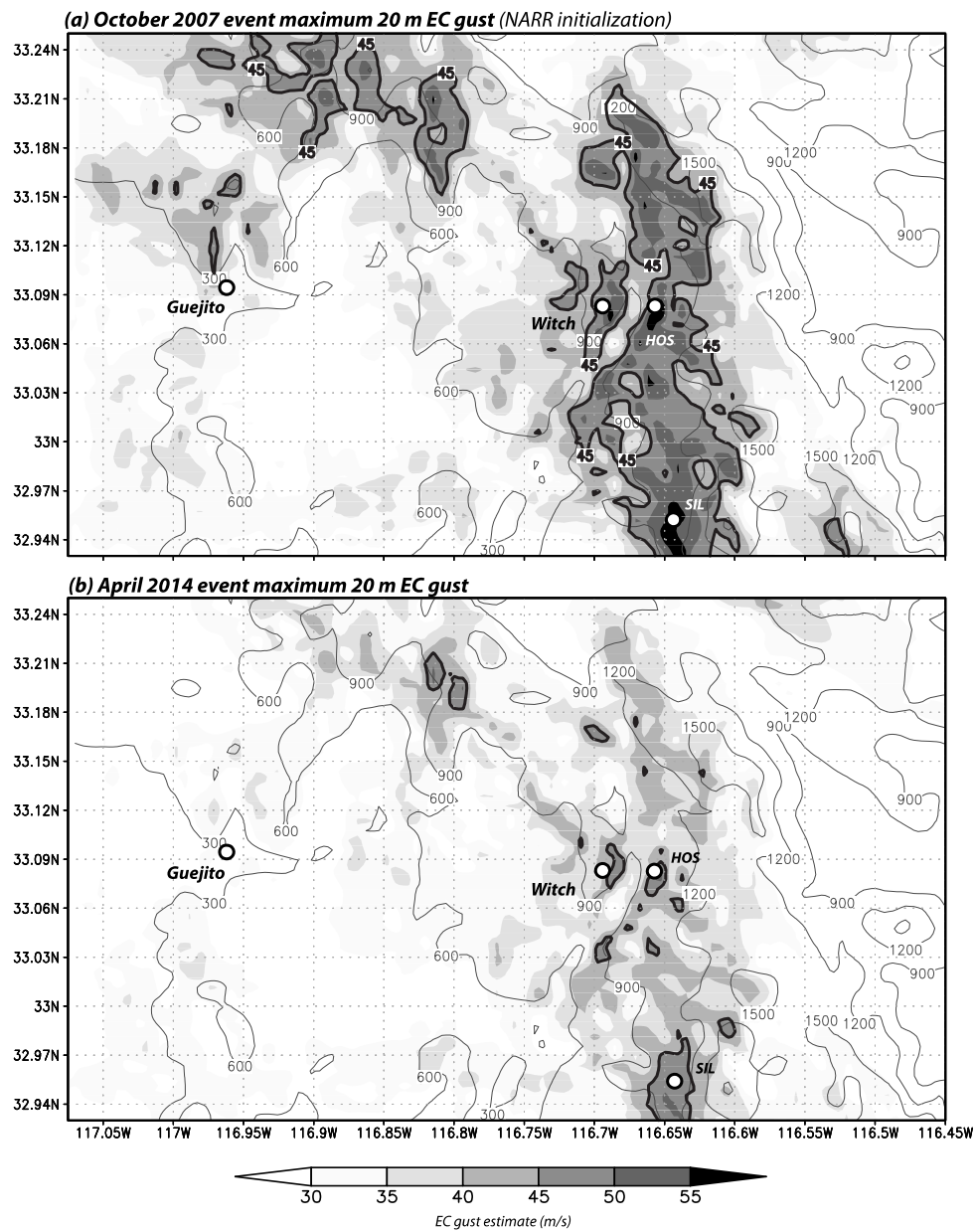
Fig. 21 Maximum simulated 20-m AGL EC gust map (shaded) for the (a) October 2007 (NARR-based run), and (b) April 2014 (NAM-based run) events. Topography (elevation from MSL) is contoured at 300-m intervals (light grey). The thick black contour highlights gusts greater than 45 m s^{-1} (100 mph). Ignition points of October 2007 Witch and Guejito fires are marked

Fig. 21 presents the event maximum gusts at the 20-m level computed using the EC formula for the October 2007 (NARR-based run) and April 2014 episodes for part of the SDG&E network. This estimate is not expected to be accurate at every single location, but suffices to illustrate the wind patterns and permit qualitative comparisons among events. The pattern of the two events is very similar, being determined by wind direction and topography, but relative to the April 2014 episode, it is seen that the October 2007 maximum gusts were likely not only more intense, but also more widespread. During the latter, the very strongest winds (exceeding 55 m s^{-1}) appeared in three places: very near the Witch ignition site, at the location of the present SDG&E station Hoskings Ranch (HOS, installed December 2013), and near SIL. The thick black contour highlights gusts ≥ 45 m s^{-1} (100 mph), and during the 2007 event, gusts that strong are also placed close to the ignition point of the Guejito fire, which broke out at 0900 UTC on October 22nd, around the event peak.

7. Maximum winds and vertical wind profiles for various Santa Ana wind events

Each Santa Ana wind event produces downslope winds with somewhat different characteristics and intensity, and with considerable temporal variation. A rough gauge of the relative strength of each event may be ascertained from comparisons of maximum winds or gusts (e.g., Fig. 21), irrespective of the time at which the maxima actually occurred. In a similar manner, Fig. 22 presents event-maximum winds in vertical planes oriented west-east across WSY and SIL for five recent Santa Ana wind events, including October 2007 (from the NARR-based run) and four of the strongest episodes since the establishment of the SDG&E mesonet. Vertical profiles for selected stations in these cross-sections are presented in Fig. 23.

Among these cases, and in both cross-sections, the October 2007 flow was clearly the fastest nearly everywhere along the lee slope. The largest values (about 41-42 m s^{-1}) are seen immediately above WSY and HOS, and near SIL (Fig. 22). Note that, unlike farther up and down the slope, the strong flows at those locations reside fairly close to the surface, and could be expected to be transported relatively easily to the ground by turbulent motions. These wind-favored locations are clearly determined by the terrain profile, as they appear (albeit with weaker wind speeds) consistently among these events.

Recall we previously noted a concern regarding the applicability in complex terrain of the logarithmic wind profile (Eq. 1), which we use to estimate the anemometer-level winds from the lowest model level $z = Z_a$ and, as a consequence, played an important role in our model verification and calibration. Specifically, the log profile is presumed valid within the surface layer, generally regarded as the lowest ~10% of the PBL depth. This is part of a larger issue regarding how well PBL schemes operate in mountainous areas. Boundary layer depths vary with time and among events, but averaged roughly 600 m at the times of maximum winds at WSY and SIL, so 10% of that is 60 m, which exceeds Z_a. It might be instructive to see if the model produces a logarithmic wind profile above $z = Z_a$ and, if so, over what depth.

Fig. 24 compares instantaneous profiles of the horizontal wind at WSY and SIL, representing the time at which the near-surface winds were at maximum for several major Santa Ana wind events. Also shown (as dashed curves) are the logarithmic wind profiles (again neglecting the zero-plane displacement) computed using (Eq. (1)). The PX LSM employs roughness lengths of 0.18 and 0.87 m, respectively, for the two sites, and static conditions were indeed neutral so ψ_{obs}, $\psi_a \sim 0$. All profiles are scaled with respect to the wind speed at the lowest model level (V_a); this renders the logarithmic profile a function of z_0 only.
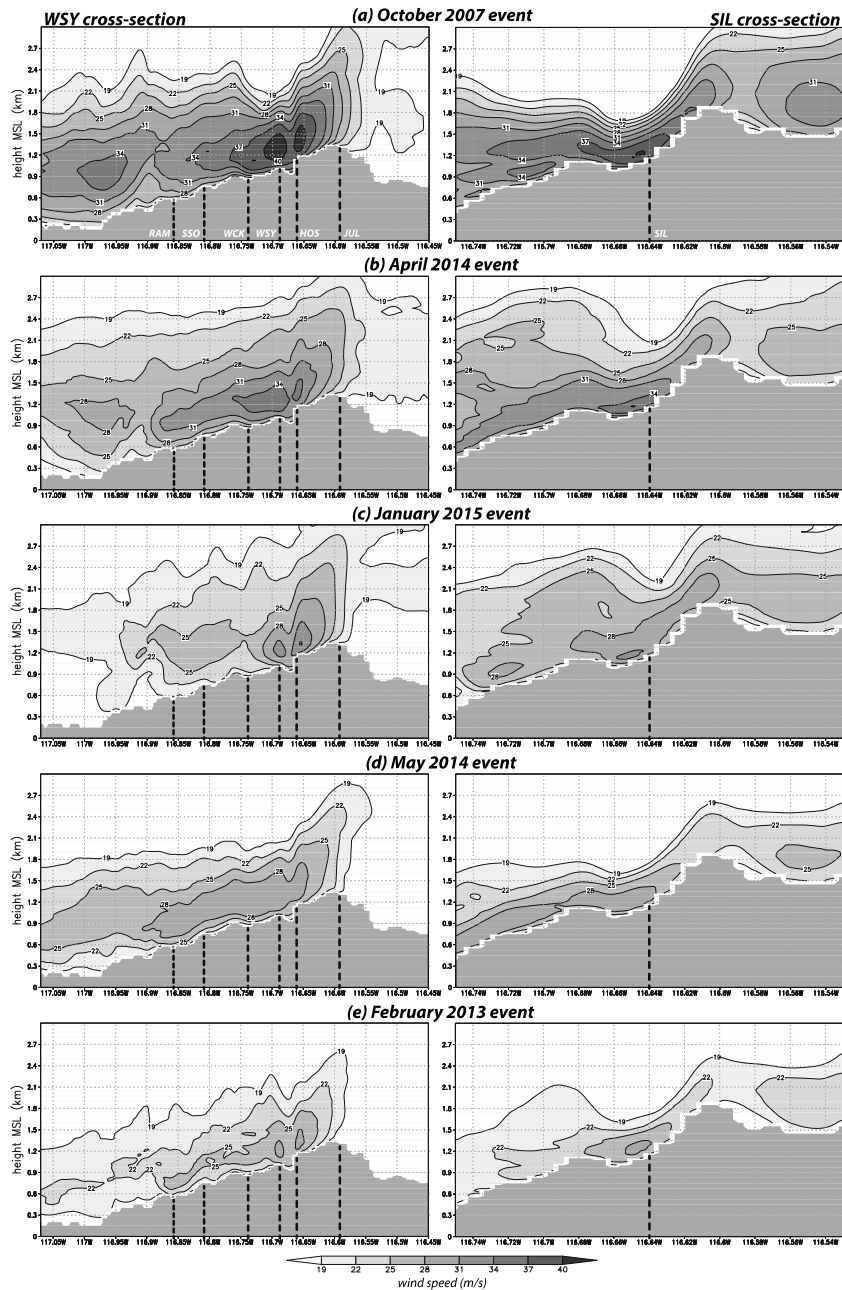
Fig. 22 West-east vertical cross-sections (longitude on abscissa) across WSY (left) and SIL (right) of event maximum winds (m s^{-1}), irrespective of occurrence time, for the (a) October 2007 (NARR-based), (b) April 2014, (c) January 2015, (d) May 2014, and (e) February 2013 events, with topography in grey. Height is above MSL. Some of the locations in the WSY section reside slightly out of the plane depicted. Note the SIL cross-sections span a smaller horizontal distance
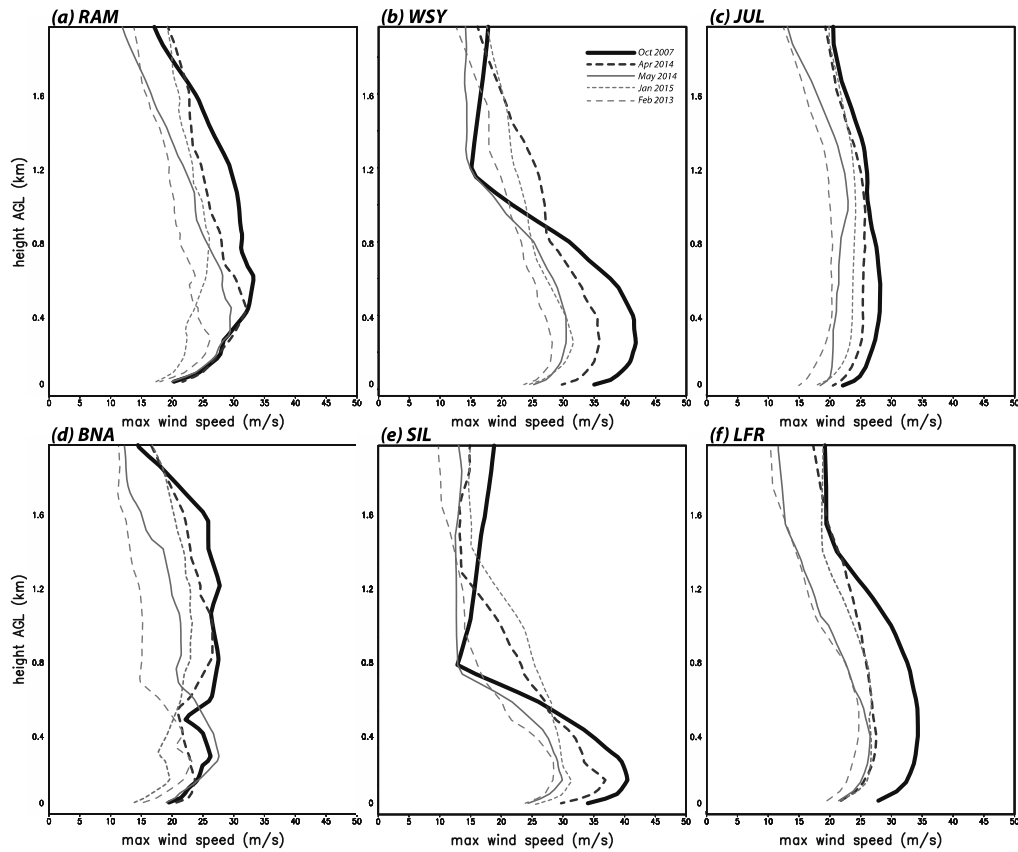
Fig. 23 Vertical profiles over the lowest 2 km AGL of event-maximum horizontal winds at six locations for the October 2007, February 2013, April and May 2014, and January 2015 Santa Ana wind events. As event maxima, the wind speeds shown at each height may not represent a single time for each event and location

Although wind speeds vary substantially, the *normalized* profiles for each station look very similar among the events. For WSY, the log profile fits the simulated winds relatively well, over at least the lowest 100 m. This might suggest that extending the log profile downward from V_a to the anemometer-level wind is reasonable. At SIL, however, the log fit to 6.1 m implies too much vertical shear. This might perhaps suggest that the surface is being treated as too rough at this location[***] and the LSM-assigned roughness value of 0.87 m does appear to be excessive for this landscape. Recall that the model substantially underforecasts winds at SIL, so employing a less rough surface in this area of the model domain might mitigate the negative forecast bias.

[***] Inclusion of a zero-plane displacement of a few meters would not change the slope of the profile, which is the issue here.

8. Conclusions

The Santa Ana winds occur in Southern California between September and May, when high pressure builds in the Great Basin (cf., Raphael 2003, Jones *et al*. 2010), reversing the normally westerly wind direction so desert air can intrude into the Los Angeles Basin. The winds have characteristics of terrain gap and/or downslope winds at various places through the region (cf. Hughes and Hall 2010, Jackson *et al*. 2013). We have examined the horizontal, vertical and temporal structure of the winds using a numerical model verified and calibrated against an exceptionally dense network of surface stations in San Diego County, operated by the San Diego Gas and Electric (SDG&E) utility. The model configuration selected did the best job of reproducing the winds at anemometer level (6.1 m AGL) over a variety of Santa Ana wind events (cf., Cao and Fovell 2016).

Three episodes were selected for closer examination herein. Two (occurring during April and May 2014) were motivated by the observational record at SDG&E stations at West Santa Ysabel (WSY) and Sill Hill (SIL), the former sited relatively close to the ignition point of the October 2007 Witch fire, and the latter representing the windiest spot in the mesonet. Along with the February 2013 Santa Ana studied by Cao and Fovell (2016), those cases were among the strongest windstorms that have occurred during the relatively short history of the SDG&E network at WSY and SIL (see Table 1). During those events, the sustained winds were strong and gust factors (the ratio between instantaneous gusts and temporally-averaged sustained winds) were higher than average for those stations.

Simulations of those and other recent events have been able to capture the network-averaged sustained winds well with respect to strength and temporal variation, albeit with systematic biases at a subset of locations. The sustained winds at both over- and underpredicted stations were likely influenced by landforms that were not resolvable, even on the highest resolution grid (667 m) employed. WSY, located in a well-exposed, largely treeless area, was one of the best-handled sites, while the reconstructed winds at SIL were far too slow. One of the factors that might account for the severe underprediction at SIL is the presence of a steep slope very near the station that does not appear on the model grid; in a similar fashion, there is a sharp terrain depression near the Witch fire site that contrasts with the more level landscape near WSY, 0.6 km away to the northeast.

Statistics for WSY and SIL showed that the frequency of strong gusts is highest between 1500-1800 UTC, which is in the morning hours after sunrise in San Diego. During those hours in the April 2014 episode simulation, an absolutely unstable layer formed over WSY, possibly supporting turbulence that could help generate particularly strong winds and convey them to the surface as gusts. Rather than a consequence of surface heating alone, this instability also resulted from differential cold advection associated with a cold, desert air mass pushing through the terrain gap to the east of the Santa Ysabel area. The unstable layer at WSY was about 200 m deep, extending up to the level where horizontal wind speeds were the highest, and the WSY record gust (still current at this writing) occurred at this time, along with a very large gust factor (> 2.0). One might expect that instability driven by surface heating would be largest during the afternoon hours, but the winds and gusts tended to be weaker then because the temperature difference across the mountains is typically smaller.

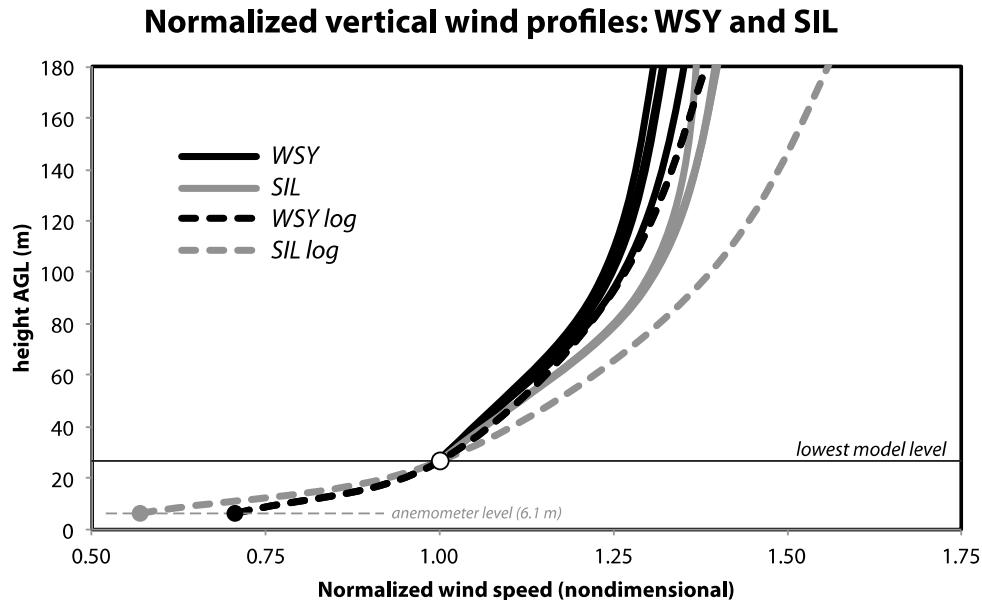**Normalized vertical wind profiles: WSY and SIL**

Fig. 24 Vertical profiles of instantaneous horizontal wind speed at WSY (solid black) and SIL (solid grey) for four Santa Ana wind events (October 2007, February 2013, and April and May 2014). Profiles were taken at times representing the maximum wind speed at about 300 m AGL for each event and time. Each profile has been scaled relative to the wind speed at the first model level above the surface (about 27 m AGL). Black and grey circles denote 6.1-m winds estimated using the log wind profile. Dashed curves indicate the logarithmic wind profiles for the two sites, presuming neutral stability and employing surface roughness lengths assigned by the LSM

The third event was the historically dramatic Santa Ana episode of late October 2007 that produced the Witch fire and over twenty other blazes. The event likely produced the strongest winds in the last half-century or so across a large portion of the region, but available observations were few in number, some questionable in quality (Cao and Fovell 2016, Fovell 2012), and all rather far removed from the fire ignition site. As in the April 2014 episode, and for the same reasons, an absolutely unstable layer formed over the Witch site during the period in which the power lines were observed to be arcing. Based on gust factors observed during April 2014, gusts as large as 45 m s^{-1} could have impacted the sparking power lines, even before considering the potential influence of the aforementioned unresolved terrain depression near the ignition site.

One of the most compelling findings that have emerged from the high-density SDG&E mesonet is how much winds can vary over short distances. This observational dataset, the present study, and our previous work (Cao and Fovell 2016, Cao 2015, Fovell and Cao 2014, Cao and Fovell 2013, and Fovell 2012), combine to demonstrate that great care is required in the estimation of winds and gusts at specific locations from observations at sites located even relatively nearby, and/or from incompletely calibrated simulations, especially those employing coarser resolution. Simulations can also be very sensitive to model physics, initialization, and even small perturbations. This applies not only to winds at particular heights, such as at anemometer level, but also as a function of height.

Table 1 Santa Ana episodes ordered by event-maximum gusts at WSY and SIL, for observations ending 31 May 2015. Original measurements were made in miles per hour. Gust rankings are from 197395 and 137368 observations at WSY and SIL, respectively. Fastest sustained winds at both stations occurred on 4/30/2014: 16.5 m s^{-1} at WSY (1610 UTC) and 31.7 m s^{-1} at SIL (1720 UTC)

Date	Time (UTC)	3-sec gust (m/s)	10-min sustained wind (m/s)	Gust factor	Gust observation ranking
WSY					
4/30/14	1600	33.5	15.7	2.14	1
5/14/14	1130	28.2	16.1	1.78	2
12/15/13	1530	27.3	16.1	1.69	6
2/15/13	1800	25.9	15.2	1.71	12 (tie)
1/24/15	1640	25.9	15.2	1.71	12 (tie)
12/9/13	1810	25.0	13.0	1.93	24
SIL					
4/30/14	1710	45.2	29.5	1.53	1
2/15/13	1820	40.7	20.6	1.98	24
1/24/15	1530	39.8	25.0	1.59	35
1/15/14	0530	39.3	22.8	1.73	39
5/13/14	1200	38.9	22.4	1.74	45 (tie)
11/25/14	0710	38.9	27.3	1.43	45 (tie)

Acknowledgments

References

Aboshosha, H. and A. El Damatty (2015), "Dynamic response of transmission line conductors under downburst and synoptic winds", *Wind Struct.*, **21**(2), 241-272.

Arakawa, A. and Lamb, V. R. (1977), "Computational design of the basic dynamical processes of the UCLA general circulation model", *Methods in Computational Physics: Advances in Research and Applications*,

17, 173-265.

Brasseur, O. (2001), Development and application of a physical approach to estimating wind gusts", *Mon. Weather Rev.*, **129**, 5-25.

Cao, Y. (2015), "The Santa Ana winds of Southern California in the context of fire weather", Ph.D. dissertation, University of California, Los Angeles, Los Angeles, California, USA.

Cao, Y. and Fovell, R.G. (2013), "Predictability and sensitivity of downslope windstorms in San Diego County", *Proceedings of the 15th Conference on Mesoscale Processes*, Portland, OR, American Meteorological Society, https://ams.confex.com/ams/15MESO/webprogram/Paper228055.html

Cao, Y. and Fovell, R.G. (2016), "Downslope windstorms of San Diego County. Part I: A Case Study", *Mon. Weather Rev.*, **144**, 529-552. http://dx.doi.org/10.1175/MWR-D-15-0147.1

Chang, C.H. and Schoenberg, F.P. (2011), "Testing separability in marked multidimensional point processes with covariates", *Ann. Inst. Stat. Math.*, **63**, 1103-1122.

Conil, S. and Hall, A. (2006), "Local regimes of atmospheric variability: A case study of Southern California", *J. Climate*, **19**, 4308-4325.

Deacon, E. L. (1955), "Gust variation with height up to 150 m", *Q. J. Roy. Meteor. Soc.*, **81**, 562-573.

Durran, D. R. (1986), "Another look at downslope windstorms. Part I: The development of analogs to supercritical flow in an infinitely deep, continuously stratified fluid." *J. Atmos. Sci.*, **43**, 2527–2543.

Fovell, R.G. (2012), "Downslope windstorms of San Diego county: Sensitivity to resolution and model physics", *Proceedings of the* 13th WRF Users Workshop, Boulder, CO, Nat. Center for Atmos. Res. https://www.regonline.com/AttendeeDocuments/1077122/43389114/43389114_1045166.pdf

Fovell, R.G. and Cao, Y. (2014), "Wind and gust forecasting in complex terrain", *Proceedings of the 15th WRF Users Workshop*, Boulder, CO, Nat. Center for Atmos. Res. http://www2.mmm.ucar.edu/wrf/users/workshops/WS2014/extended_abstracts/5a.2.pdf

Huang, C., Lin, Y.L., Kaplan, M.L. and Charney, J.J. (2009), "Synoptic-scale and mesoscale en- vironments conducive to forest fires during the October 2003 extreme fire event in Southern California", *J. Appl. Meteor. Clim.*, **48**, 553-579.

Hughes, M. and Hall, A. (2010), "Local and synoptic mechanisms causing Southern California's Santa Ana winds", *Clim. Dynam.*, **34**(6), 847-857.

Jackson, P.L., Mayr, G. and Vosper, S. (2013), Dynamically-driven winds. *Mountain Weather Research and Forecasting*, (Eds., F.K. Chow, S.F.J.D. Wekker, and B.J. Snyder), Springer-Verlag, 121-218.

Jones, C., Fujioka, F. and Carvalho, L.M.V. (2010), "Forecast skill of synoptic conditions associated with Santa Ana Winds in Southern California", *Mon. Weather Rev.*, **138**, 4528-4541.

Lou, W., Wang, J., Chen, Y., Lv, Z. and Lu, M. (2016), "Effect of motion path of downburst on wind-induced conductor swing in transmission line", *Wind Struct.*, **23**(3), 211-229.

Mesinger, F., et al. (2006), "North American regional reanalysis", *Bull. Am. Meteor. Soc.*, **87**, 343-360.

Monahan, H.H. and Armendariz, M. (1971), "Gust factor variations with height and atmospheric stability", *J. Geophys. Res.*, **76**, 5807-5818.

Pleim, J.E. (2007), "A combined local and non-local closure model for the atmospheric boundary layer. Part I: Model description and testing", *J. Appl. Meteor. Clim.*, **46**, 1383-1395.

Pleim, J.E. and Xiu, A. (1995), "Development and testing of a surface flux and planetary boundary layer model for application in mesoscale models", *J. Appl. Meteor.*, **34**, 16-32.

Raphael, M.N. (2003), "The Santa Ana winds of California", *Earth Interact.*, **7**, 1-13.

Skamarock, W.C., et al. (2007), "A description of the Advanced Research WRF Version 2", National Center for Atmospheric Research, Tech. Note NCAR/TN-468+STR, 88.

Small, I.J. (1995), "Santa Ana winds and the fire outbreak of Fall 1993", NOAA Technical Memorandum, National Weather Service Scientific Services Division, Western Region.

Smith, C.M. and Skyllingstad, E.D. (2011), "Effects of inversion height and surface heat flux on downslope windstorms", *Mon. Weather Rev.*, **139**, 3750-3764.

Sommers, W.T. (1978), "LFM forecast variables related to Santa Ana wind occurrences", *Mon. Weather Rev.*, **132**, 1307-1316.

Stensrud, D.J. (2007), *Parameterization Schemes: Keys to Understanding Numerical Weather Prediction*

Models. Cambridge University Press, Cambridge, UK.

Suomi, I., Vihma, T., Gryning, S.E. and Fortelius, C. (2013), "Wind-gust parametrizations at heights relevant for wind energy: a study based on mast observations", *Q. J. Roy. Meteor. Soc.*, **139**, 1298-1310.

Verkaik, J.W. (2000), "Evaluation of two gustiness models for exposure correction calculations", *J. Appl. Meteor.*, **39**, 1613-1626.

Vosper, S.B. (2004), "Inversion effects on mountain lee waves", *Q. J. Roy. Meteor. Soc.*, **130**, 1723-1748, doi:10.1256/qj.03.63.

Westerling, A.L., Cayan, D.R., Brown, T.J., Hall, B.L. and Riddle, L.G. (2004), "Climate, Santa Ana winds and autumn wildfires in Southern California", *Eos*, *Trans. Amer. Geophys. Union*, **85**, 289-296.

Wieringa, J. (1976), "An objective exposure correction method for average wind speeds measured at a sheltered location", *Q. J. Roy. Meteor. Soc.*, **102**(431), 241-253, doi:10.1002/ qj.49710243119.

Xiu, A. and Pleim, J.E. (2001), "Development of a land surface model. Part I: Application in a mesoscale model", *J. Appl. Meteor.*, **40**, 192-209.

Yang, F. and Zhang, H.J. (2016), "Two case studies on structural analysis of transmission towers under downburst", *Wind Struct.*, **22**(6), 685-701.